RSC Advances

REVIEW

View Article Online
View Journal | View Issue

Cite this: *RSC Adv.*, 2024, **14**, 38757

Fluorescent probes for sensing and visualizing methylglyoxal: progress, challenges, and perspectives

Jing Wen,[b] Qingya Zhang[a] and Liyi Zhou *[a]

Received 21st October 2024
Accepted 27th November 2024

DOI: 10.1039/d4ra07512a

rsc.li/rsc-advances

Methylglyoxal (MGO) plays an important role not only in physiological processes but also in pathological conditions, including diabetes, hypertension, and Alzheimer's disease. Therefore, developing accurate quantitative tools for MGO is of great significance for studying pathogenesis. Among the various methods available, the fluorescent probe method has garnered considerable attention due to its noninvasive detection capability, exceptional optical properties, good biocompatibility, and high sensitivity. In this review, we provide a brief overview of recent research on fluorescent probes used for MGO biosensing and bioimaging in living cells, tissues, and animals. Additionally, we summarize the advantages and existing challenges and also discuss future directions for development in this field.

1. Introduction

Methylglyoxal (MGO), one of the reactive carbonyl species (RCS),[1] is closely associated with physiological activities in organisms. Endogenous MGO is generated from processes such as glycolysis, lipid peroxidation and protein metabolism.[2–4] As for exogenous resources, MGO can be formed in foods *via* the Maillard reaction. Hence, it is common to find MGO in thermally processed foods, especially those rich in carbohydrates.[5,6] Besides, MGO can modify substances like proteins, DNA and others, so it is regarded as a major precursor of advanced glycation end products (AGEs). MGO is not only of relevance to hyperglycemia but also involved in vascular complications, which indicates its effects on diabetes. Likewise, numerous studies point out that abnormal levels of MGO and AGE formation can cause several malignant diseases, including diabetes,[7,8] hypertension[9,10] and Alzheimer's disease.[11,12] However, the specific pathogenic mechanisms of MGO are not clear. Therefore, accurate quantitative MGO tracking techniques are needed for further studies.

Until now, traditional techniques used for MGO detection include high-performance liquid chromatography,[13] liquid chromatography-mass spectrometry,[14] capillary electrophoresis,[15] and electrochemical approaches.[16] Nevertheless, these procedures typically require the destruction of the cell structure or are performed using dead cells. In addition, they are limited by high cost, inadequate samples, and variability in detection that needs a long reaction time, making them unsuitable for real-time exogenous and endogenous MGO monitoring. Recently, considerable research efforts have been devoted to detecting MGO concentrations in living cells *via* newly constructed fluorescent probes due to their nondestructive examination methods and high sensitivity.

Prior studies have either reported the single designed approaches or comparisons with the conventional detecting techniques. In 2022, Jana *et al.*[17] reviewed a series of fluorescent probes used for quantifying and visualizing reactive carbonyl species. Many researchers have also focused on the study of formaldehyde (FA).[18] In contrast, there is no systematic review of MGO fluorescent sensors. This review focuses on the development and application of fluorescent probes for MGO detection in the past 10 years and classifies the probes into four categories based on their reactive sites. Furthermore, *o*-phenylenediamine-based probes that can be combined with new techniques are further compared and summarized. In the end, the prospect and future directions are contemplated. This review will provide a reference for further studies on the construction of innovative fluorescent probes for MGO detection and imaging, thereby promoting their innovative applications in the diagnosis and assessment of related diseases (Scheme 1).

2. Design strategies for fluorescent probe construction and their response mechanisms

With the development of spectral technology, fluorescence imaging with chemical probes has received considerable interest in the biomedical field.[19–21] Fluorescent probes are

[a]*College of Food Science and Engineering, Central South University of Forestry and Technology, Changsha, Hunan 410004, China. E-mail: zhouly0817@163.com*
[b]*School of Food Science and Technology, Hunan Agricultural University, Changsha, Hunan 410125, China*

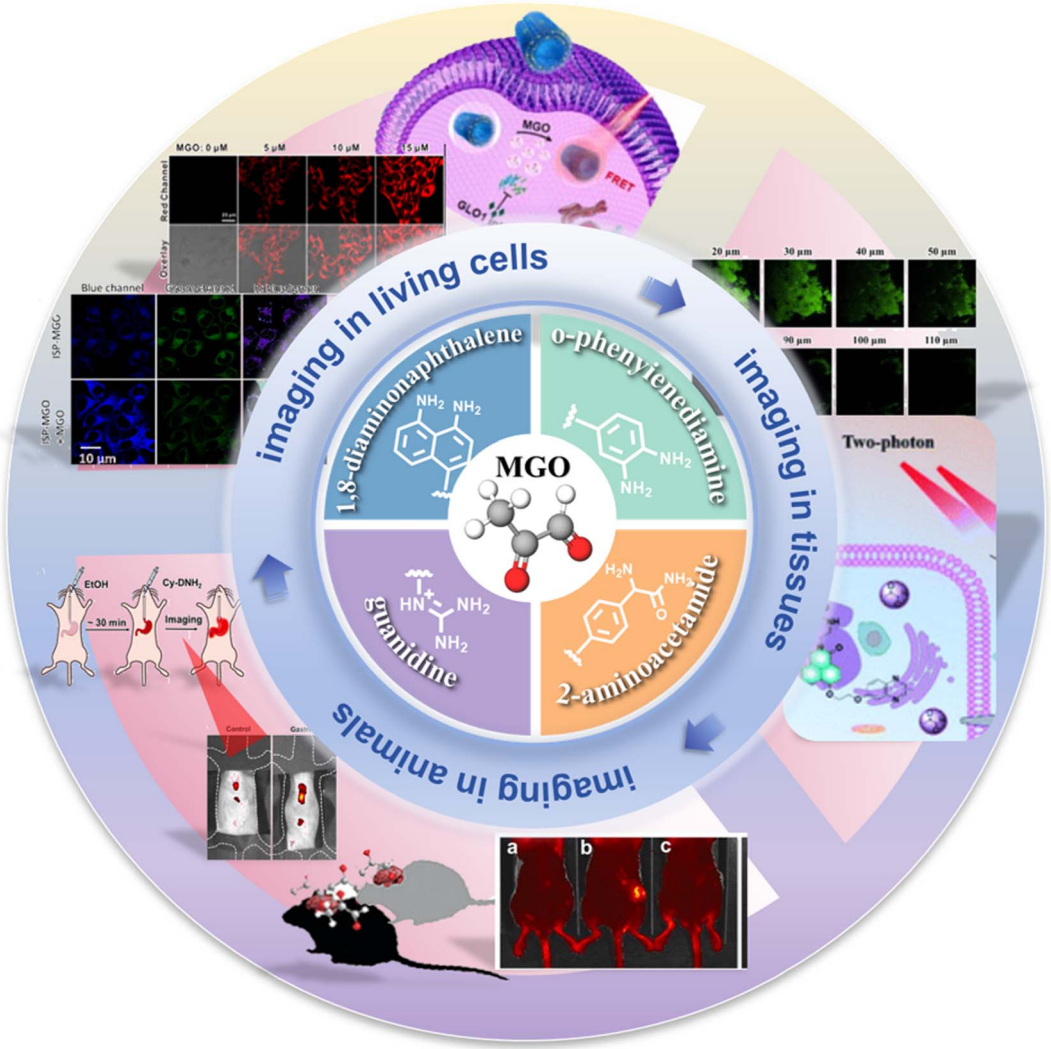

Scheme 1 Schematic representation of fluorescent probes used for MGO detection.

applied not only for sensing substances but also in bio-imaging. Probe types usually include "turn-on" probes and ratiometric probes. According to relevant reports,[17,22] numerous RCS fluorescent probes have been invented in the past few years. To date, their common response mechanisms include but are not limited to photoinduced electron transfer (PET), intramolecular charge transfer (ICT), and Förster resonance energy transfer (FRET).

PET-based fluorescent probes comprise three parts, an electron-deficient fluorophore that acts as an electron acceptor,[23] a receptor that functions as a fluorophore quencher and provides an electron, and a spacer that links the fluorophore and the receptor. When electrons are transferred from the donor to the acceptor, the charge transfer process consumes the excited state energy of the fluorescent substance, resulting in fluorescence quenching. However, in the presence of the target, it reacts with the receptor, and the PET effect is destroyed, resulting in fluorescence enhancement.[24] On the other hand, two or more groups with different electronic affinities exist in an ICT-based fluorescent probe. Charge transfer between the excited and ground states produces different emission colors in different environments.[25] The FRET effect is based on a non-radiative energy transfer process. The excited fluorophore realizes energy transfer depending on its distance from the receptor. When a fluorophore acts as the receptor, the obtained energy is released during fluorescence emission, and the molecule is reverted back to the ground state.[26,27] Researchers have used the fluorescence changes enabled by these mechanisms to achieve qualitative and quantitative analysis. These effects are widely used in physics, chemistry, biology, and other fields, and have been widely studied and utilized. The specific mechanisms are explained below using examples.

3. Fluorescent probes for MGO detection

Many probes are synthesized such that they undergo a specific reaction with MGO. Based on distinct identification groups at

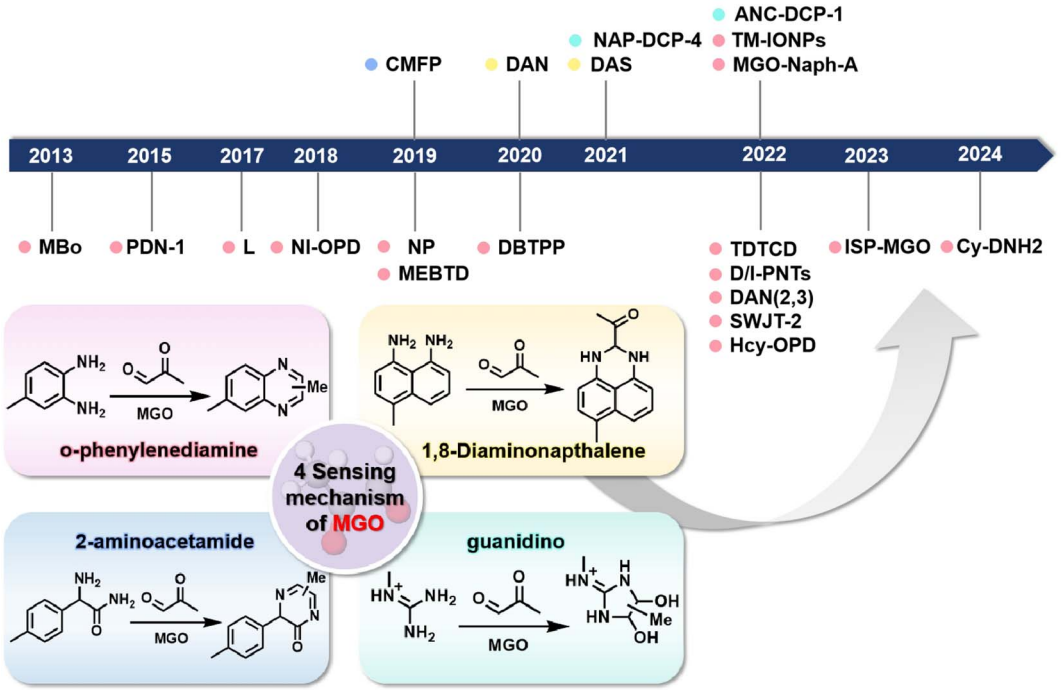

Fig. 1 Schematic of the sensing mechanisms depending on the four different identification groups and the development timeline of the fluorescent probes of MGO.

the reactive site, the currently developed fluorescent probes for MGO tracing can be divided into 4 categories: *o*-phenylenediamine (OPD), 2-aminoacetamide, 1,8-diaminonaphthalene, and guanidino (GND), as shown in Fig. 1. The synthesis and application of these probes are discussed individually below, in the same order.

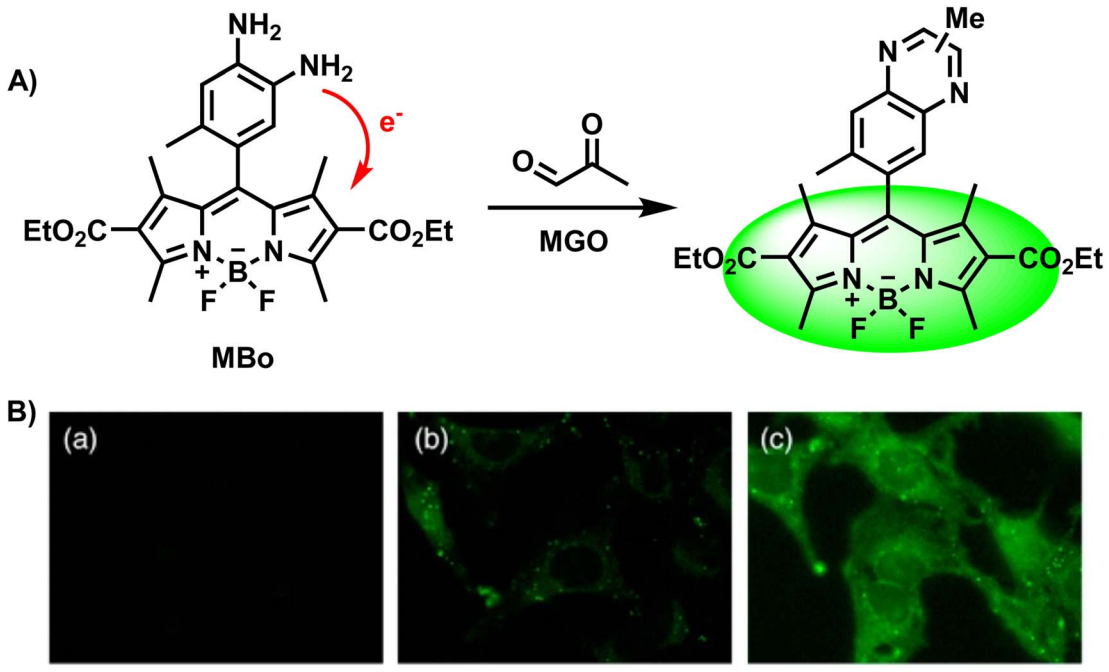

Fig. 2 (A) Recognition mechanism of MBo. (B) Fluorescence images of live HeLa cells stained with MBo. This figure has been reproduced from ref. 28 with permission from the American Chemical Society, copyright 2024.

3.1. *O*-Phenylenediamine

Because of the reaction between MGO and *o*-phenylenediamine, researchers first attach the OPD moiety to various fluorophores, and OPD reacts with MGO irreversibly to form methylquinoxalines. Currently, a variety of fluorescent probes for MGO detection have been developed and synthesized using the *o*-phenylenediamine unit as the recognition group. Considering that OPD also reacts with NO, a step to test selectivity is required to validate the newly developed probe. Typically, researchers measure and contrast the fluorescence response results of the constructed probe to MGO, reactive carbonyl species, reactive oxygen/nitrogen species, metal ions and other substances, respectively.

In 2013, Spiegel *et al.*[28] assembled BODIPY and OPD to construct the first fluorescent "turn-on" probe called MBo, which was successfully employed to detect and image MGO in biological samples (Fig. 2A). Based on photoinduced electron transfer (PET), one of the common working principles of fluorescent probes, the fluorescence was quenched by using a boron-dipyrromethene (BODIPY) fluorophore as the electron acceptor and *o*-phenylenediamine as the electron donor. Considering that only quinoxaline has appropriate HOMO/LUMO levels to module the a-PET (acceptor-excited PET) and d-PET (donor-excited PET) processes, they discussed the effects of different substituents and selected the 6-methyl substituent. Thus, the fluorescence quantum yield obtained was ten times the original when MBo was combined with MGO, showing an increase from 0.003 to 0.326 with obvious responses. After 1 h incubation in PBS, the LOD of the reported probe was 50–100 nM. Because the scaffold MBo was first designed to detect NO, they also considered and finally evidenced the selectivity of MBo. Its imaging capacity was also examined, as shown in Fig. 2B.

After two years, Tang *et al.*[29] designed a two-photon "turn-on" fluorescent probe, PDN-1 (Fig. 3A), which was a naphthalimide derivative and exhibited great penetrability, which was evident from the fluorescence signal output (more than 600 nm). PDN-1 was incubated in a PBS solution with and without MGO, respectively. This probe turned "on" in tandem with a significant increase in one-photon fluorescence intensity, and showed a linear relationship as the concentration of MGO was increased. On the other hand, the PET effect first dampened the fluorescence. With a detection limit of 77 nM, PDN-1 demonstrated exquisite sensitivity and continues to hold the record for the lowest LOD among two-photon fluorescent probes used to monitor MGO, to the best of our knowledge. Furthermore, the imaging studies conducted in HeLa cells validated its application potential for tracking MGO in live cells (Fig. 3B).

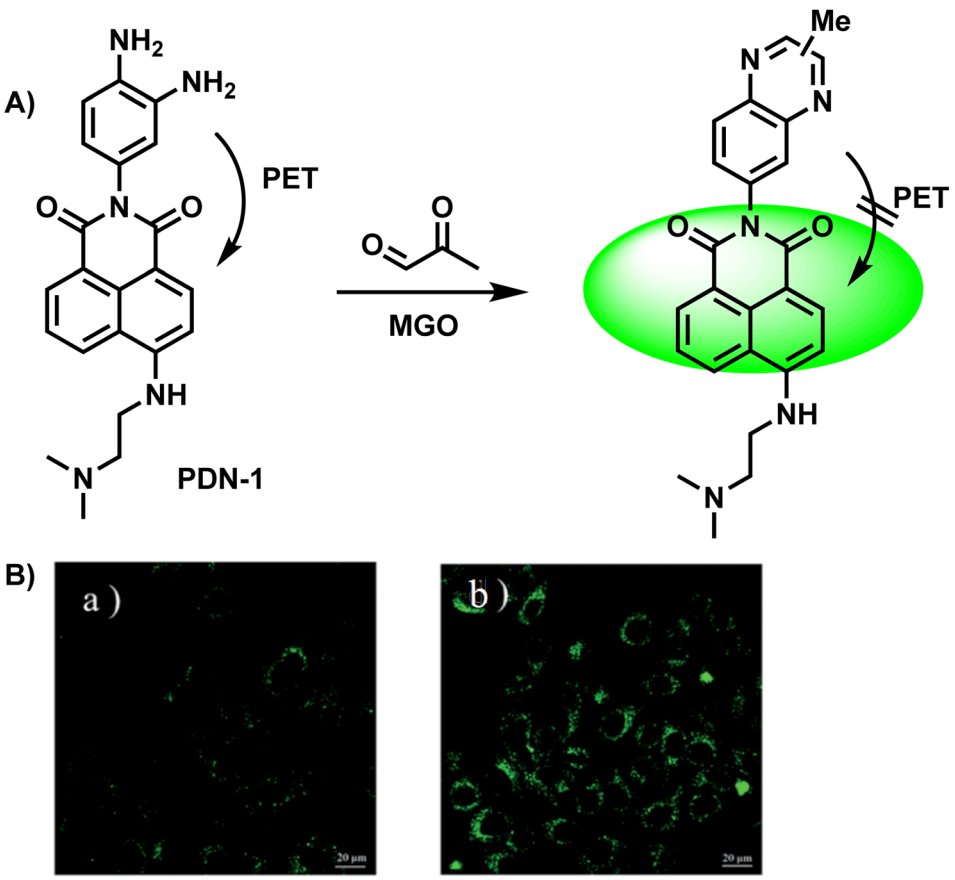

Fig. 3 (A) Recognition mechanism of PDN-1. (B) Fluorescence imaging of live HeLa cells by PDN-1 with 10 nM and 100 nM MGO. This figure has been reproduced from ref. 29 with permission from the Royal Society of Chemistry, copyright 2015.

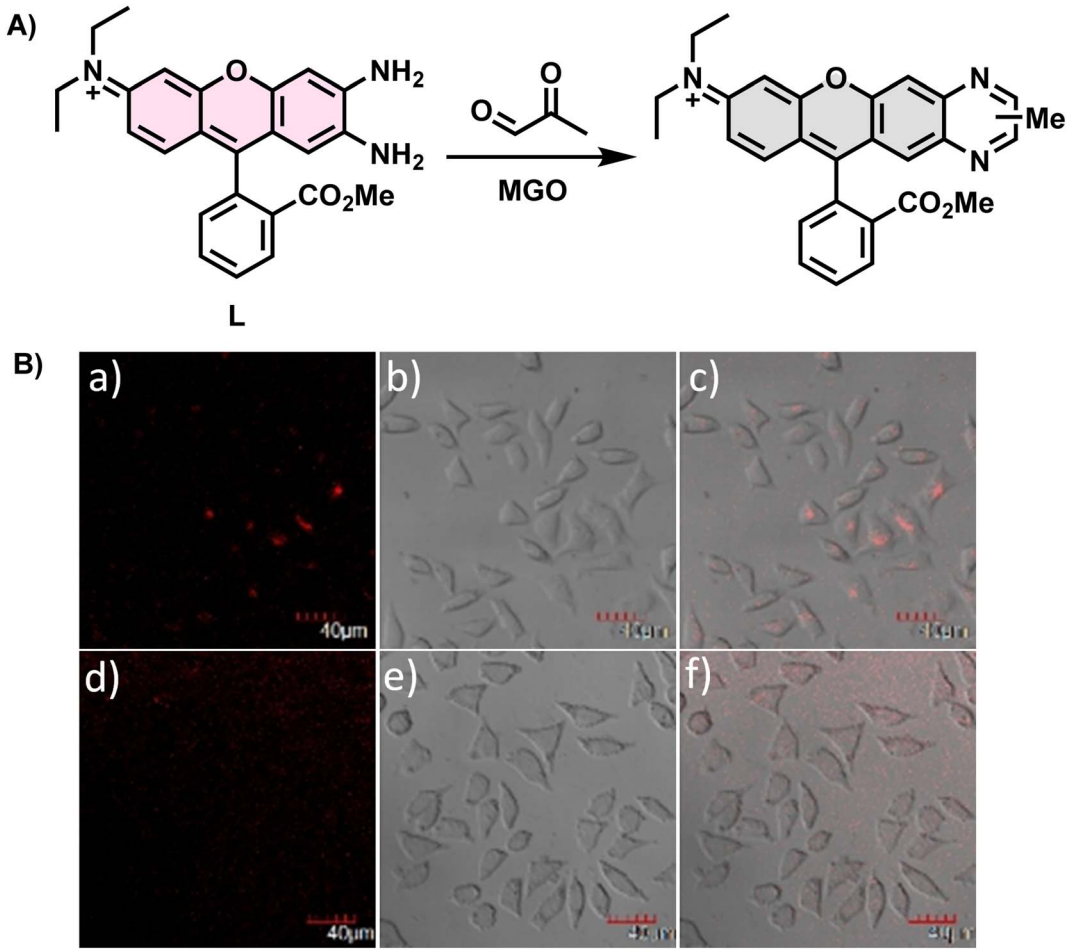

Fig. 4 (A) Recognition mechanism of L. (B) Fluorescence imaging of L929 cells incubated with L. This figure has been reproduced from ref. 30 with permission from Elsevier, copyright 2017.

In 2017, Liu *et al.*[30] utilized an *ortho*-diamino rhodamine derivative as a novel probe named L (Fig. 4A), which could not only measure MGO in complex mixtures containing alkyl/aromatic aldehydes, diacetyl, amino acids, and other compounds but also detect formaldehyde (FA) and oxalaldehyde (OA) by changing the emission patterns. When only the probe was present, the fluorescence intensity of the peak at 642 nm was weak. On the contrary, after the addition of FA, MGO, and OA, a change was observed in the corresponding intensity or wavelength. Therefore, it could discriminate these analytes from other substances that caused no significant effects. During detection, as the concentration of MGO increased, the fluorescence was progressively quenched, leading to a reduction in the quantum yield of L to half of its initial value. Imaging of living cells indicated that L possessed cell permeability (Fig. 4B). Based on the validated reactions between L and the analytes, this technique is expected to be used more widely in the future.

In 2018, Yang *et al.*[31] synthesized NI-OPD, an endoplasmic reticulum-targeting fluorescent probe, which was successfully applied in quantitative imaging of endogenous MGO in a diabetic mice model (Fig. 5A). Along with a two-photon 1,8-naphthalimide moiety as the fluorophore, it contained OPD as the identification group. Due to the interaction between MGO and OPD in the probe, the PET effect was restrained, resulting in intense fluorescence emission. NI-OPD hardly produced fluorescence by itself. On the contrary, when the content of MGO reached 30 μM, the fluorescence quantum yield was about 75-fold higher than the control group because of the formation of the 2-methylquinoxaline product NI-MQL. Cell imaging tests not only focused on differentiating the normal and diabetic mice but also quantified the MGO level in sick mice after metformin (Metf) treatment (Fig. 5B). The fluorescence in their kidney and liver tissues significantly decreased after a 7 days medication therapy, in line with expected outcomes, proving the suitability of NI-OPD in sensing MGO.

Gao *et al.*[32] developed a new two-photon probe NP, which effectively detected and imaged MGO levels in cells, tissues and zebrafish (Fig. 6A). Due to the initial presence of PET, there was no fluorescence release in the control group. Nevertheless, with the addition of MGO, the PET effect was blocked and a bright green fluorescence signal was obtained, which was also verified by the spectral response, that is, a fluorescence intensity peak occurred at 555 nm when the concentration of MGO reached

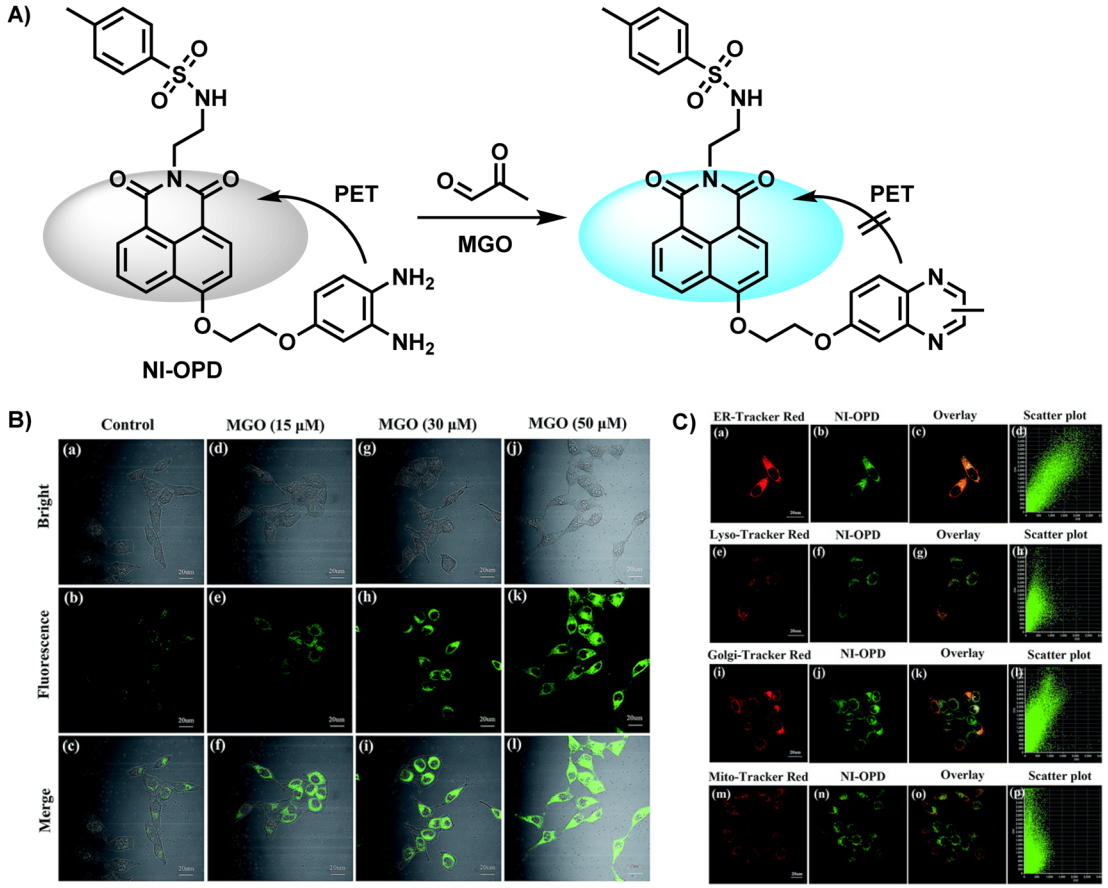

Fig. 5 (A) Recognition mechanism of NI-OPD. (B) Fluorescence imaging of HeLa cells using NI-OPD with distinct concentrations of MGO. (C) Colocalization images of HeLa cells stained with NI-OPD. This figure has been reproduced from ref. 31 with permission from the Royal Society of Chemistry, copyright 2018.

150 μM. Compared with the obvious response caused by the condensation–cyclization reaction, the NO-induced weak fluorescence was negligible. Due to its little toxicity and notable enhancement of green channel fluorescence, NP demonstrated viability for MGO detection and imaging in HeLa cells in both one- and two-photon modes (Fig. 6B), as well as zebrafish and liver tissue.

Dang *et al.* developed a near-infrared (NIR) fluorescent probe (DBTPP) featuring a thiadiazole-fused OPD moiety for receptor detection (Fig. 7A).[33] Owing to the generation of MTQPP, which is the quinoxaline product of DBTPP and MGO, solutions changed color under a UV light from light green to red when excited at 500 nm (Fig. 7B and C). The probe showed excellent selectivity by producing considerably higher fluorescence compared to various other substances that may affect the effect of DBTPP fluorescence response. In addition, DBTPP was successfully applied not only to quantify the *in vivo* and *ex vivo* MGO levels in SH-SY5Y cells but also for imaging endogenous MGO in a transgenic AD mouse model.

In eukaryotic cells, many organelles play important roles in biological metabolism. Nevertheless, organelle-targeting fluorescent probes are rarely reported. Probes with organelle-targeting characteristics can be designed by assembling the targeting chemical group. In 2022, Luo *et al.*[34] designed MGO-Naph-A, a lysosome-targeting fluorescent probe, by combining naphthalimide with OPD, which functioned as the fluorophore and recognition group, respectively (Fig. 8A). The PET effect was constrained during the reaction of OPD and MGO, resulting in strong fluorescence emission. In the presence of MGO, two new peaks appeared at 340 mm and 400 mm, and the fluorescence quantum yield increased to 87.03 from the initial value of 9.25. A linear relationship was observed between fluorescence intensity and the amount of MGO added ($R^2 = 0.992$) in the concentration range of 0–90 mM (Fig. 8B). The corresponding limit of detection was 1.36 μM. Selectivity experiments proved that the probe could discriminate MGO from aldehyde species, including formaldehyde (FA) and glyoxal (GO). Normally, to further demonstrate the feasibility of the probe in MGO detection, researchers utilize the MGO scavenger *N*-acetylcysteine (NAC) for capturing endogenous MGO in a pretreatment step, and test cytotoxicity by the MTT assay to ensure that the probe meets the basic conditions of cell imaging. Equipped with morpholine as the lysosome-targeting group, MGO-Naph-A exhibited lysosomal localization, as shown in Fig. 8C. Besides, the zebrafish fluorescence imaging experiment proved its validity *via* contrast tests, illustrating its application potential.

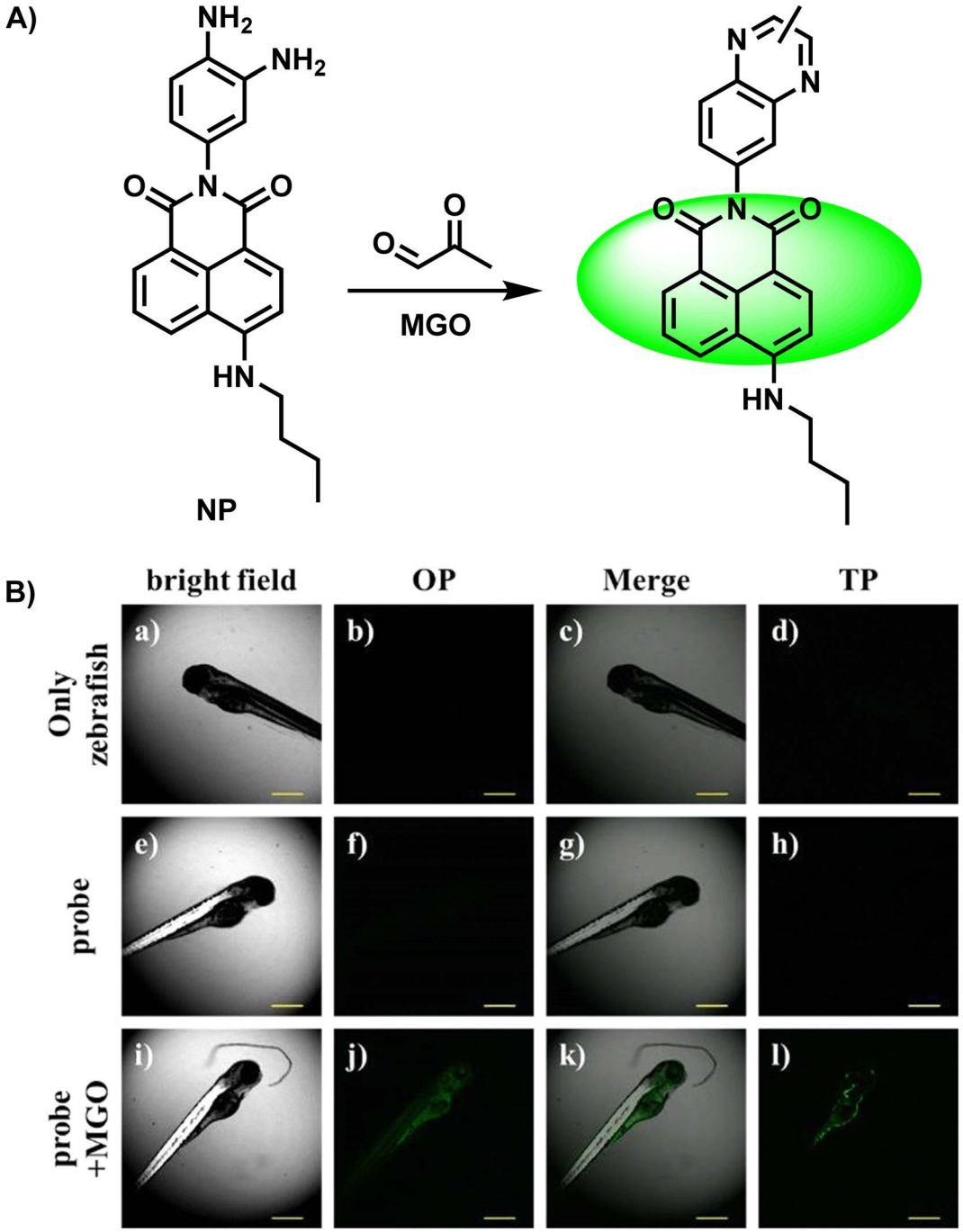

Fig. 6 (A) Recognition mechanism of NP. (B) Fluorescence imaging of zebrafish using NP in the presence and absence of MGO. This figure has been reproduced from ref. 32 with permission from Springer, copyright 2018.

Compared to probes with emission in the visible region, those with emission in the second near-infrared region owing to low SBRs usually encounter less interference and can penetrate deeply into tissues. In light of this, Dang *et al.* developed a NIR-II fluorescent nanoprobe (TDTCD) that could also use OPD as the recognition group.[35] When incubated in a solution with relatively weak polarity (chloroform and EA), the color shift that occurred two minutes after the addition of MGO was more prominent than that in the polar microenvironment. However, two days after the addition, the color of all sample solutions changed to a dark shade, as seen in Fig. 9. Consequently, after further analysis, Dang's group employed lecithin and solid PCMs to provide a nonpolar environment for TDTCD in order to speed up the response time. The obtained MGO-activatable NIR-II fluorescent nanoprobe, MG-SLNP, exhibited an LOD of 57 nM in PBS. Unlike previously reported probes that were often stable in neutral and slightly alkaline conditions, the fluorescence signal of this novel probe was unaffected at pH values

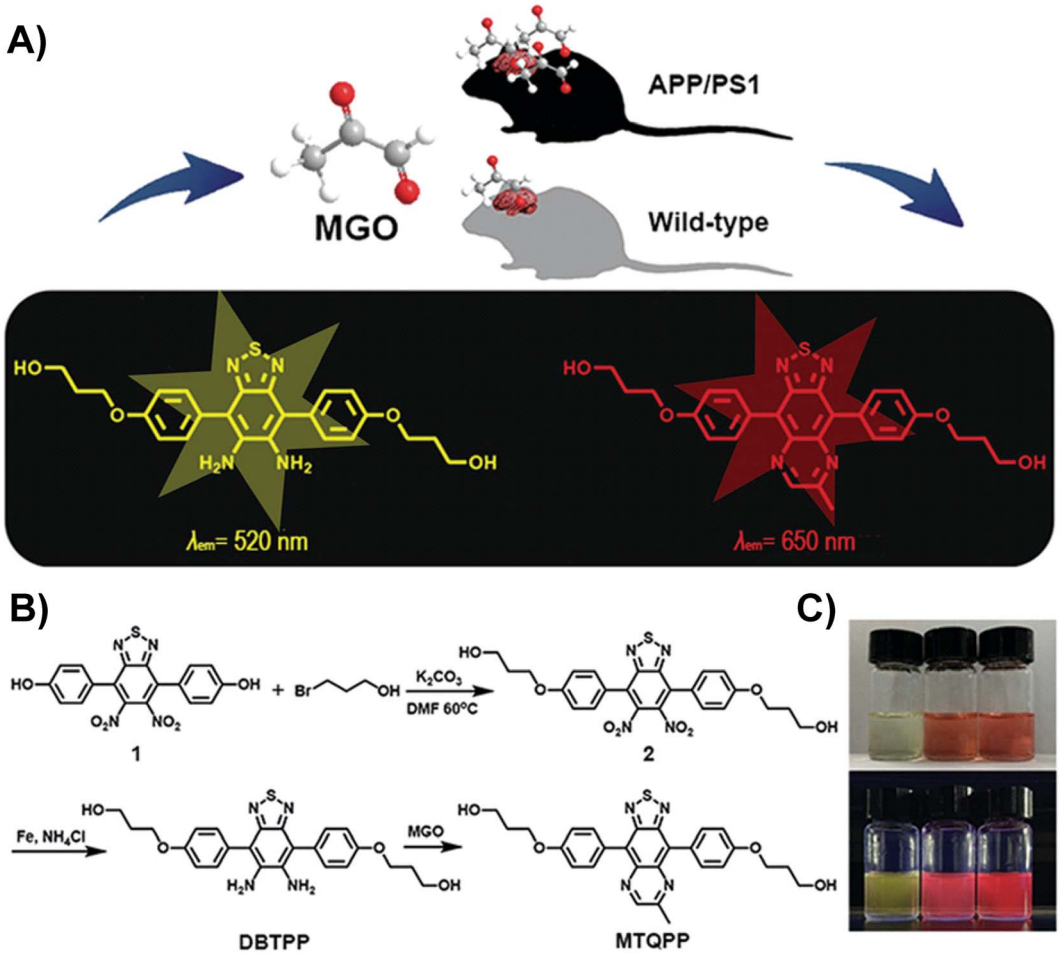

Fig. 7 (A) Schematic of DBTPP. (B) Synthesis of DBTPP. (C) Photos of solutions under visible light (upper) and UV light (lower). From left to right: DBTPP, DBTPP + MGO, and MTQPP. This figure has been reproduced from ref. 33 with permission from the Royal Society of Chemistry, copyright 2019.

ranging from 4.0 to 8.5. This indicates enormous potential for the widespread use of this probe. Unfortunately, although TDTCD could be applied for MGO analysis in mice and whole blood and consumed less time than the traditional HPLC technique, the poor penetrability limited its imaging ability in the type-2 diabetes model, which provided the ideas for improvement in subsequent research.

In the same year, their research group reported another novel NIR-II fluorescent nanoprobe, M-IONPs, for quantifying and imaging MGO, which proved significant for the diagnosis of early Alzheimer's disease (AD).[36] The nanoprobe exhibited great binding affinity to the Fe_3O_4 nanoparticle surface and penetrability, producing emission in the NIR-II region. Benefitting from PEGylated phospholipid coating, TM-IONPs revealed further enhanced permeability (Fig. 10). Because of this structure, TM-IONPs were able to overcome the complicated blood–brain barrier (BBB) and enter the brain, enabling AD diagnosis. With a good linear relationship and a detection limit of 210 nM, the absorbance signal at 500–900 nm rose with the steady increase in MGO concentration from 0.25 to 30 μM, causing a color shift from light yellow to green. From the *in situ* NIR-II imaging of MGO variations in the brains of AD mice, a 24.2-fold fluorescence enhancement was observed in mice brains after treatment, demonstrating the effectiveness of the probe. The analysis of AGEs in the AD brain and anastomosis was facilitated by imaging MGO, which was the precursor of AGEs, also demonstrating the association of MGO and AD disease, as MGO has been proven to be related to protein cross-linking and oxidative stress.

Different from fluorescent probes that provide only a single emission feature, ratiometric fluorescence probes are well-resistant to environmental and other target-independent interference as they allow detection by comparing the fluorescence ratios at two or more different wavelengths before and after the reaction.[37,38] In 2023, Liang *et al.*[39] reported a ratiometric fluorescent probe, ISP-MGO, for detecting and imaging MGO (Fig. 11A). With the help of an ethenylene unit, OPD was linked with the fluorophore, forming the donor–π–acceptor (D–π–A) skeleton. ISP-MGO emitted near-infrared fluorescence at 700 nm in phosphate-buffered solution when 415 nm was used as the excitation wavelength. In response to the increase in MGO concentration, the intensity ratio of the 520 and 700 nm

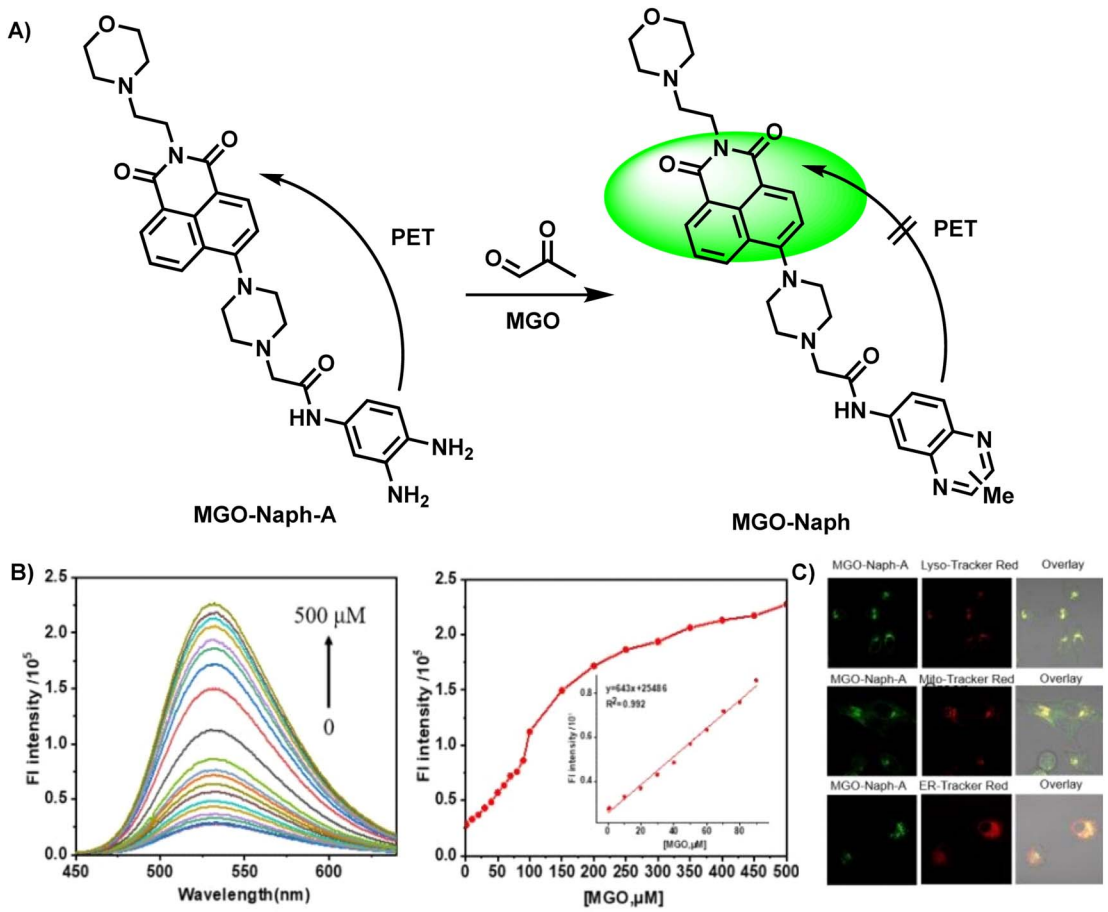

Fig. 8 (A) Recognition mechanism of MGO-Naph-A. (B) Fluorescence response of MGO-Naph-A to MGO at concentrations in the range of 0–90 μM. (C) The colocalization imaging of A549 cells stained with MGO-Naph-A. This figure has been reproduced from ref. 34 with permission from Elsevier, copyright 2022.

(I_{520}/I_{700}) peaks increased from 0.12 to 1.9. Compared with the MGO level recognized in diabetes and Alzheimer's disease patients, the excellent sensitivity was demonstrated by ISP-MGO, with a detection limit of 2.18 ± 0.12 μM, which was enough to indicate whether people were sick. The primary basis for its suitability for *in vivo* MGO quantification was established by the superior selectivity and steady I_{520}/I_{700} ratio at near-*in vivo* pH conditions. Further results of the cell imaging experiments demonstrated the feasibility of ISP-MGO in detecting MGO both *in vitro* and *in vivo* (Fig. 11B and C).

These days, a large proportion of fluorescence probes are developed to measure MGO, which is thought to be a biomarker for diabetes, the characteristic of samples from blood suggests they normally works in neutral and weakly alkaline conditions. In this regard, Xu *et al.*[40] designed and synthesized an acid-promoted fluorescent probe Cy-DNH2, which could be used to detect endogenous MGO in living cells (Fig. 12A). In this ICT-based probe, benzo[*cd*]indolium was bonded with OPD, forming a D–π–A structure. Following the addition of MGO, the specific combination of MGO and electron-rich OPD reduced the conjugation ability of the system, which led to a blue shift in wavelength. Furthermore, in acidic circumstances, the chemical enhanced fluorescence intensity at 545 nm. This probe showed sensitivity (with a low limit of detection of 95 nM) and quick responsiveness within 3 minutes, while traditional techniques usually require one to two hours. Previous studies have pointed out the importance of visualization of MGO content in inflammatory gastrointestinal cells for gastritis diagnosis. When the gastric organs of both healthy and ill mice were imaged using Cy-DNH2, the stomach with gastritis emitted a strong signal, showing its capability for gastritis diagnosis (Fig. 12B). Although fluorescent probes are capable of both sensing MGO and performing bio-imaging, it is necessary to first examine the cytotoxicity of the sensor in order to evaluate the imaging effect. Particularly, in small-molecule-based sensors, there are possibilities of leakage into the cells during the penetration process.[41] Test assays include, but are not limited to CCK-8 assay used in Xu's study and the MTT assay utilized in Luo's research.[34] Researchers can choose the optimal concentration of probes for the following stage based on the experimental results of the cell survival rate.

FRET is another traditional response mechanism of fluorescent molecular probes, besides PET and ICT. In 2022, Liu *et al.*[42] combined two probes (hydrophobic DBTPP reported in

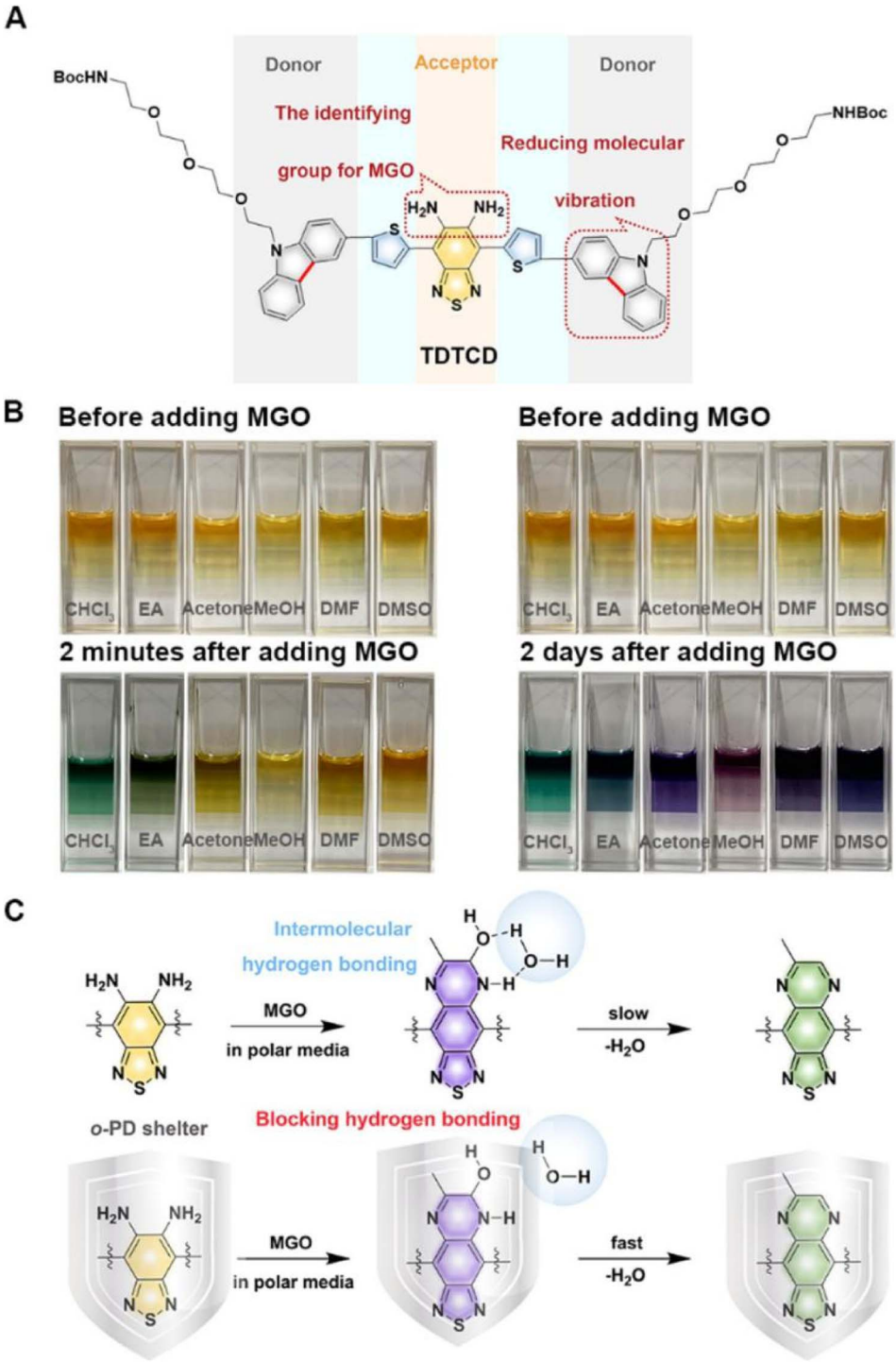

Fig. 9 (A) Structure of TCTCD. (B) Photographs of the solutions two minutes and two days after the addition of MGO. (C) Recognition mechanism of TCTCD. This figure has been reproduced from ref. 35 with permission from the American Chemical Society, copyright 2024.

2021 (ref. 33) and hydrophilic IR783) and encapsulated them in 4 nm-thick peptide nanotubes, obtaining the D/I-PNTs nanoprobe. The structure is shown in Fig. 13. As mentioned in previous studies, near-infrared probes can penetrate deeply into the tissues, which is deficient in the case of lower-wavelength excitation light.[43,44] Owing to its emission in the first near-infrared (NIR-I) region, D/I-PNTs could sense MGO in deep tissues. Compared to the absorption and emission spectra of DBTPP and MTQPP (product of the DBTPP with OPD), the response of MGO helped in increasing the emission range to 800–850 nm. Furthermore, its MGO specificity and stability in mice serum provided a strong basis for its precise visualization

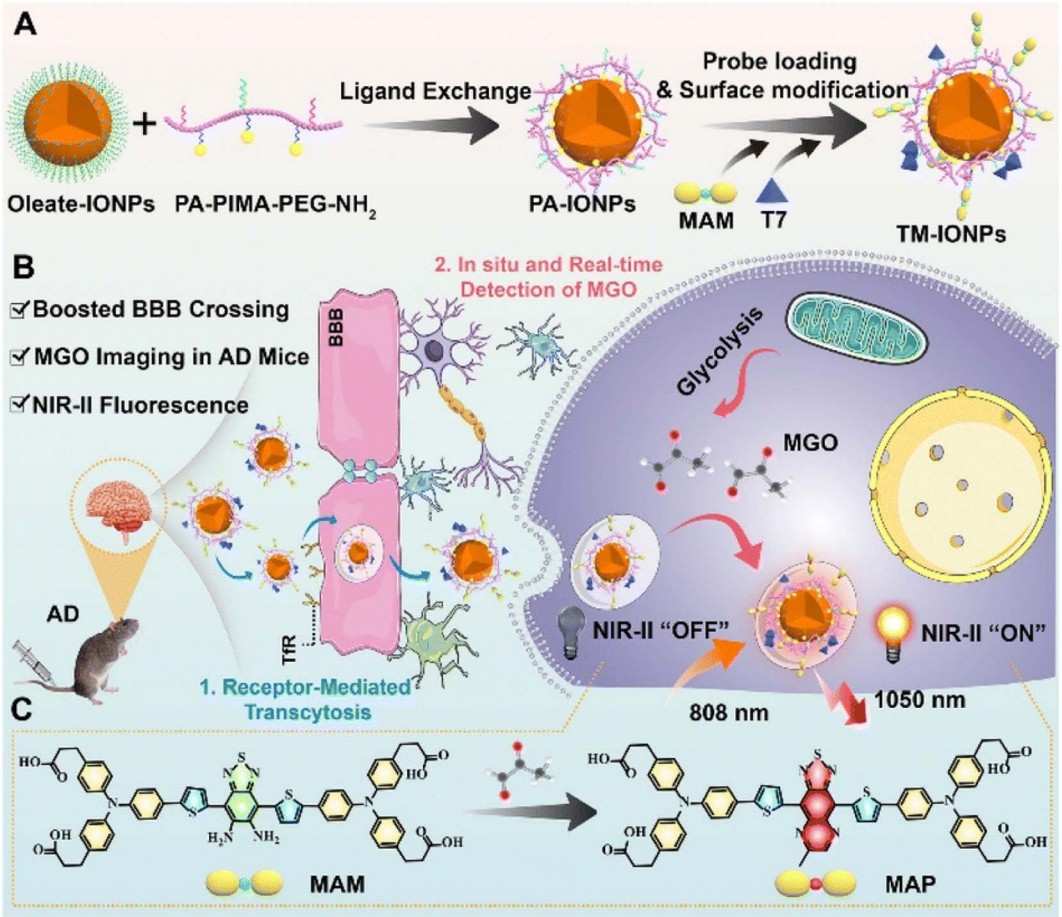

Fig. 10 (A) Synthesis of TM-IONPs. (B) Applications of TM-IONPs in living cells and the brains of AD mice. (C) Recognition mechanism of MAM. This figure has been reproduced from ref. 36 with permission from the Royal Society of Chemistry, copyright 2022.

in mice and live cells. Additionally, the universality of this nanoplatform encouraged more researchers to create innovative nanoprobes for biosensing.

In 2022, Xie *et al.*[45] utilized 2,3-diaminonaphthalene (DAN) to develop a ratiometric fluorescence MGO sensing probe, which enabled imaging of exogenous MGO in live cells, as well as *ex vivo* imaging of MGO in the tissues of type II diabetes model mice (Fig. 14A). The formation of 2-methylbenzo [*g*]quinoxaline during its reaction with OPD led to a change in fluorescence from blue to green, with an LOD of 0.33 μM. In addition, they designed MGO multicolor fluorescent test strips by fixing DAN to a filter paper such that results can be observed easily by the naked eye (Fig. 14C). This work provided a convenient and simple tool for on-site rapid detection of MGO.

Although there is endogenous production of MGO, the enzymatic systems in human bodies will help in degrading it and keeping the MGO at the normal levels.[4,46] MGO detoxification usually happens with the help of the glyoxalase system, which comprises 2 enzymes, namely GLO1 and GLO2. However, according to relevant reports, there is a relationship between high GLO1 expression and tumor progression.[47] Therefore, the *in vivo* MGO levels indirectly indicate GLO 1 enzyme activity. Ding's team[48] invented MEBTD, a novel NIR fluorescence probe, which could be used for MGO visualization in tumors, with a low LOD of 18 nM for MGO. This probe featured a D–A–D structure; however, owing to the inducement of MGO, a newly generated thiadiazole-fused quinoxaline planar motif became the new electron acceptor, resulting in a novel electronic push–pull system and alteration of the fluorescent signal. When the MGO content was increased to 50 μM, the MEBTD fluorescence at 650 nm in PBS surprisingly increased by 131 times compared with the control group. As illustrated in Fig. 15B, the 4T1 cell mean fluorescence intensities assessed using various methods indicated a 35-fold and 42-fold increase in values with an increase in MGO concentration from 0 to 15 μM. The imaging results revealed that MEBTD could image the MGO content *in vivo* and assess the impact of GLO1 inhibitors.

In addition to the examples mentioned above, there are probes based on reaction structure similar to OPD, and the difference lies mainly in the reaction site being the secondary amine rather than the primary amine in OPD. A novel near-infrared fluorescent probe named SWJT-2 was reported by Xu's group in 2022 (Fig. 16A).[49] SWJT-2 was constructed based on the dicyanoisophorone derivative. The absorption and fluorescence increased when SWJT-2 interacted with MGO at pH = 7.4, and the fluorescence quantum yield varied from 0.003

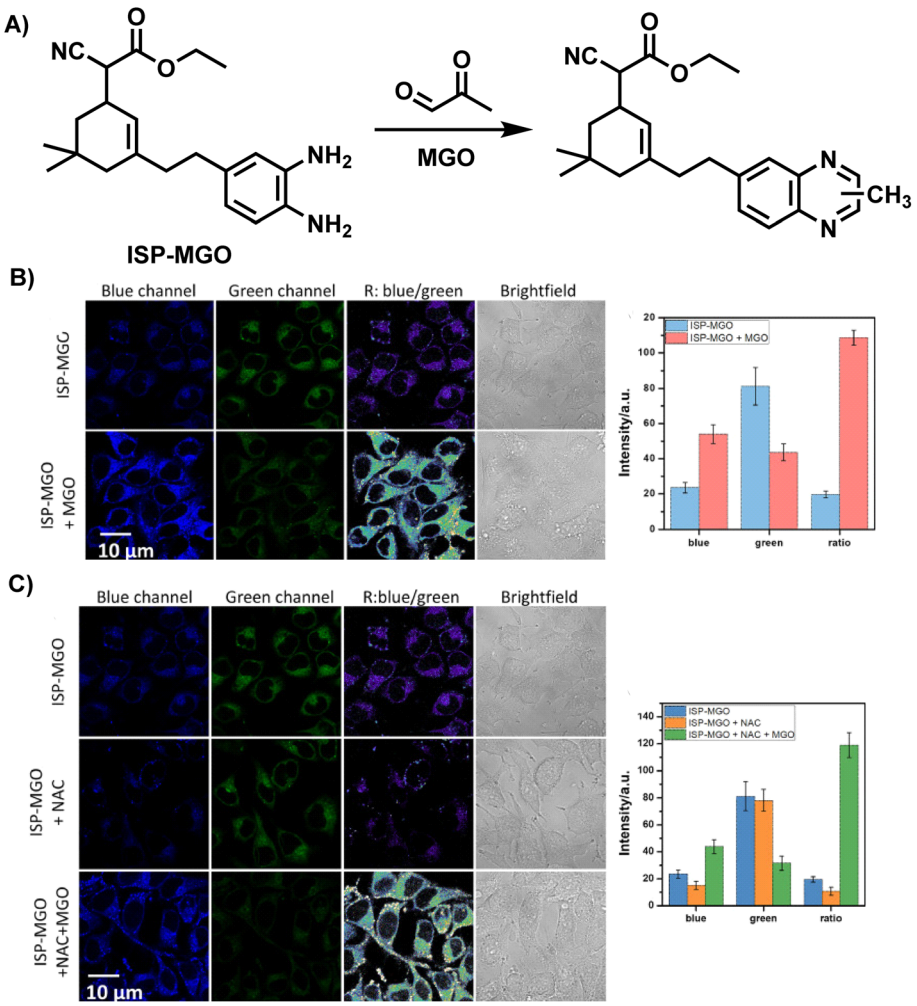

Fig. 11 (A) Recognition mechanism of ISP-MGO. (B) Fluorescence imaging of HeLa cells using ISP-MGO with/without MGO. (C) Fluorescence imaging of HeLa cells with *in vivo* MGO using ISP-MGO. This figure has been reproduced from ref. 39 with permission from Elsevier, copyright 2024.

(initial) to 0.015. The fluorescence intensity and MGO concentration were linear in the range of 0 to 10.0 μM, with a computed detection limit of 0.32 μM. Notably, the reaction process only took 15 minutes since the secondary amine was selected as the recognition site, significantly reducing the amount of time required and making real-time detection a reality.

Similarly, Wang's group introduced a pre-organized isopropylamino group into the Hcy-OPD probe to modulate its selectivity by increasing the hindrance effect (Fig. 17A).[2] The experimental results showed that fluorescence at 658 nm was greatly enhanced, and the intensity of the red channel was increased to 3 times the original after MGO addition (Fig. 17B). The linear range of emission intensity at this wavelength and MGO concentration was 0–0.8 mM, with a LOD of 0.22 μm. In the specificity assays, the presence of alkyl/aromatic aldehydes and amino acids did not interfere with the detection result. Additionally, the existence of NO did not affect the fluorescence. On the other hand, the results obtained with Mito-Tracker Green agreed well with the red channel of Hcy-OPD in the study of subcellular distribution, proving the mitochondria-targeting capability of this probe (Fig. 17C). Researchers in the above two examples changed the primary amine structure and improved the properties of probes. This type of probe can be seen as a subbranch of OPD-based probes. The secondary amine enabled SWJT-2 to react rapidly, while Hcy-OPD showed higher selectivity with the enhancement of the hindrance effect. However, there are few relevant researches. More examples must be explored to understand whether the secondary amines in modified can expedite the process of detection in the human body or improve the properties of the probes.

Advances in science and technology have led to the development of new fluorescent probes that are more accurate, sensitive, and cause less damage to cells during detection.[50] This section has addressed most types of fluorescent probes that were designed to take advantage of the irreversible reaction of OPD and MGO. These can be further divided into groups based on the kinds of probes used. Several common

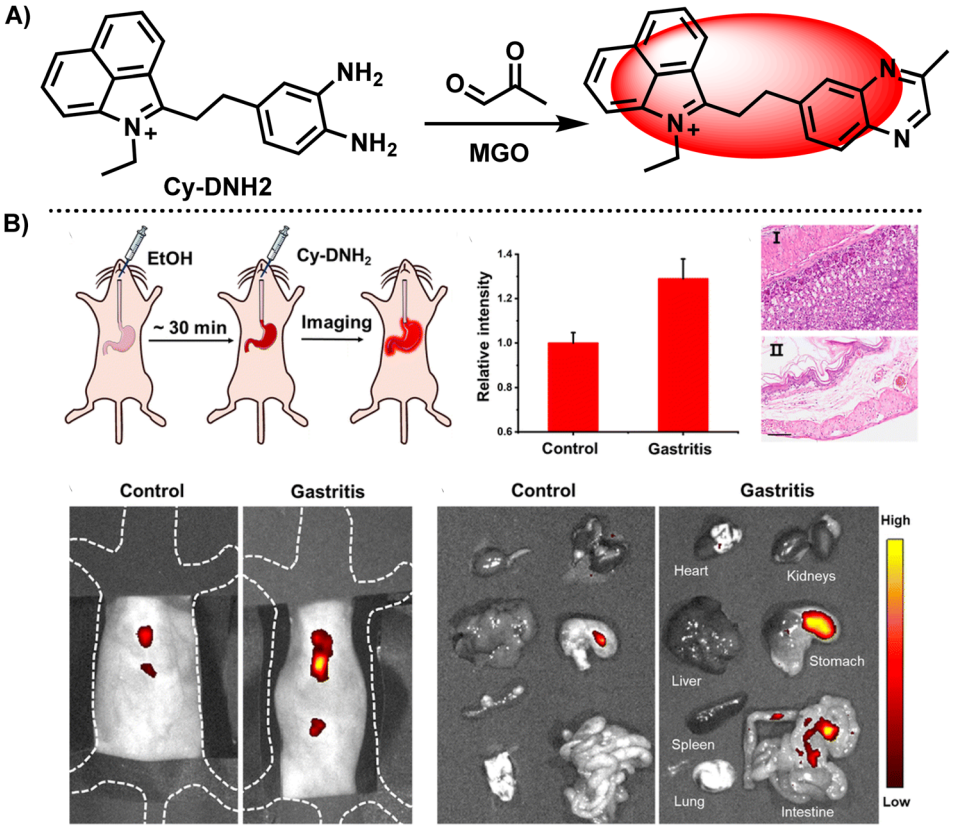

Fig. 12 (A) Recognition mechanism of Cy-DNH2. (B) Fluorescence images of the control and gastritis mouse models using Cy-DNH2. This figure has been reproduced from ref. 40 with permission from the Royal Society of Chemistry, copyright 2024.

types include "turn-on", "turn-off", two-photon, ratiometric and near-infrared fluorescent probes. Beyond all doubt, there are advantages and shortcomings to different probe types. For instance, the first "turn-on" MGO probe inspired a number of researchers to design new probes based on this fluorescence response. Besides, following Liu *et al.*, the "turn-off" manner was utilized for detection and visualization by others.[30] Nevertheless, these probes are vulnerable to the external environment in practical applications. Considering that, the ratiometric methods stand out extraordinarily as a result of less interference from the detection environment and larger Stokes shift compared to the single fluorophore strategy. The two-photon type shows good performance in terms of deep penetration, less photodamage, higher signal-to-noise ratios and low auto-fluorescence. Similarly, the near-infrared probes have great advantages, including high signal-to-noise ratio (S/N), low tissue damage, and deep tissue penetration due to their emission in the near-infrared (especially for NIR-II) region. Thus, near-infrared sensors are widely preferred. Nonetheless, there is room for these techniques to develop. Recent studies in other fields have discovered several ways to improve detection performance, opening up new possibilities for researchers in the area of biological detection.[51] It is anticipated that as the technology advances, fluorescent probes will be applied more broadly for MGO sensing and imaging.

3.2. 2-Aminoacetamide

In 2019, Wang *et al.*,[52] developed CMFP, the first ratiometric fluorescent probe, for application in clinical analysis (Fig. 18A). Based on the reaction site of 2-aminoacetamide, MGO concentrations in the range of 0–600 μM were linear with the ratio of peak intensities at 440 and 525 nm (I_{440}/I_{525}), which increased from 0.09 to 3.02 and by around 33.6-fold. With a calculated LOD of 0.24 μM, Wang *et al.*[52] considered the complexity of the actual tests so they computed the LOD in real samples (0.5 μM), which demonstrated the sensitivity of CMFP. CMFP was used for MGO detection in whole blood samples from diabetic and healthy people. Although the final data did not show a clear relationship between the fluorescence ratio and blood glucose concentration, the development of the CMFP probe provides an effective tool to quantify MGO and further investigations on the relationship between MGO and diabetes. However, further validation of CMFP is needed before formal clinical use.

3.3. 1,8-Diaminonaphthalene

In addition, except for the possibility of selecting OPD as the response group for the detection of MGO, naphthalene derivatives can also be used as the recognition group for MGO detection. Jana *et al.*[53] designed and constructed a naphthalene-based fluorescent probe called DAN (1,8-diaminonaphthalene) taking inspiration from 2,3-diaminonaphthalene,

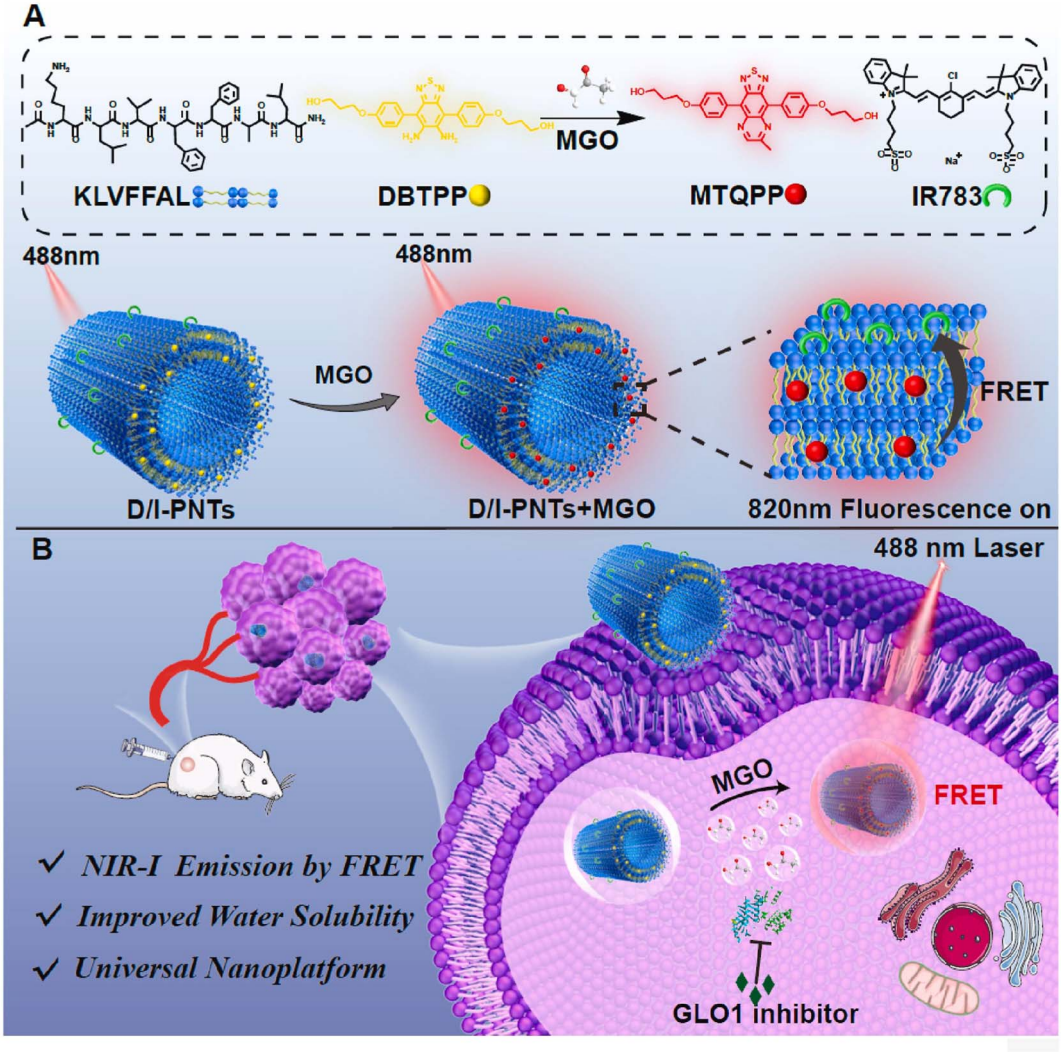

Fig. 13 (A) Recognition mechanism and schematic of D/I-PNTs. (B) Applications of D/I-PNTs in living cells and 4T1 tumor-bearing mice model. This figure has been reproduced from ref. 42 with permission from Elsevier, copyright 2024.

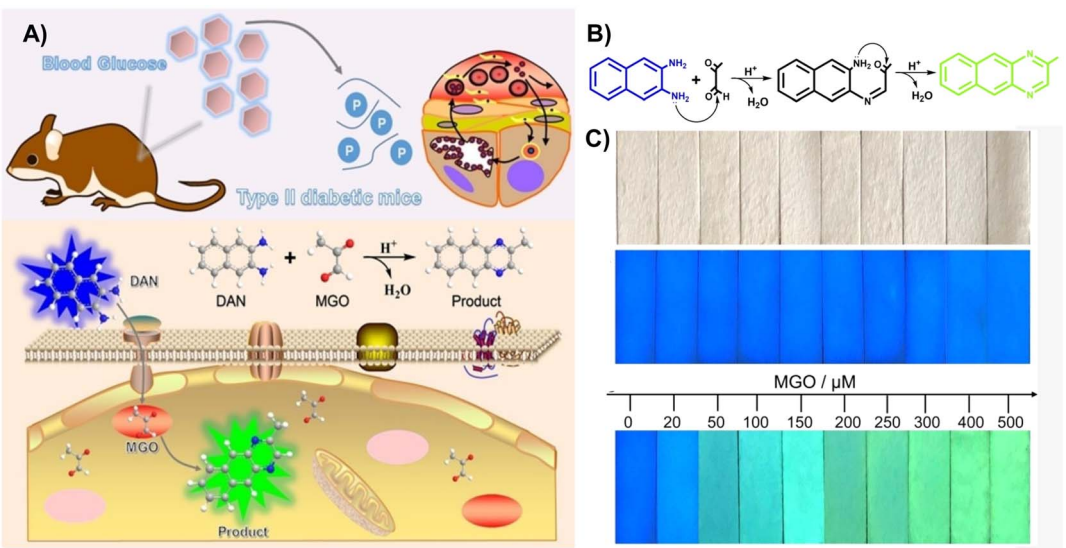

Fig. 14 (A) Schematic of DAN. (B) Recognition mechanism of DAN. (C) Color change of the invented test strips at distinct MGO levels. This figure has been reproduced from ref. 45 with permission from Wiley, copyright 2022.

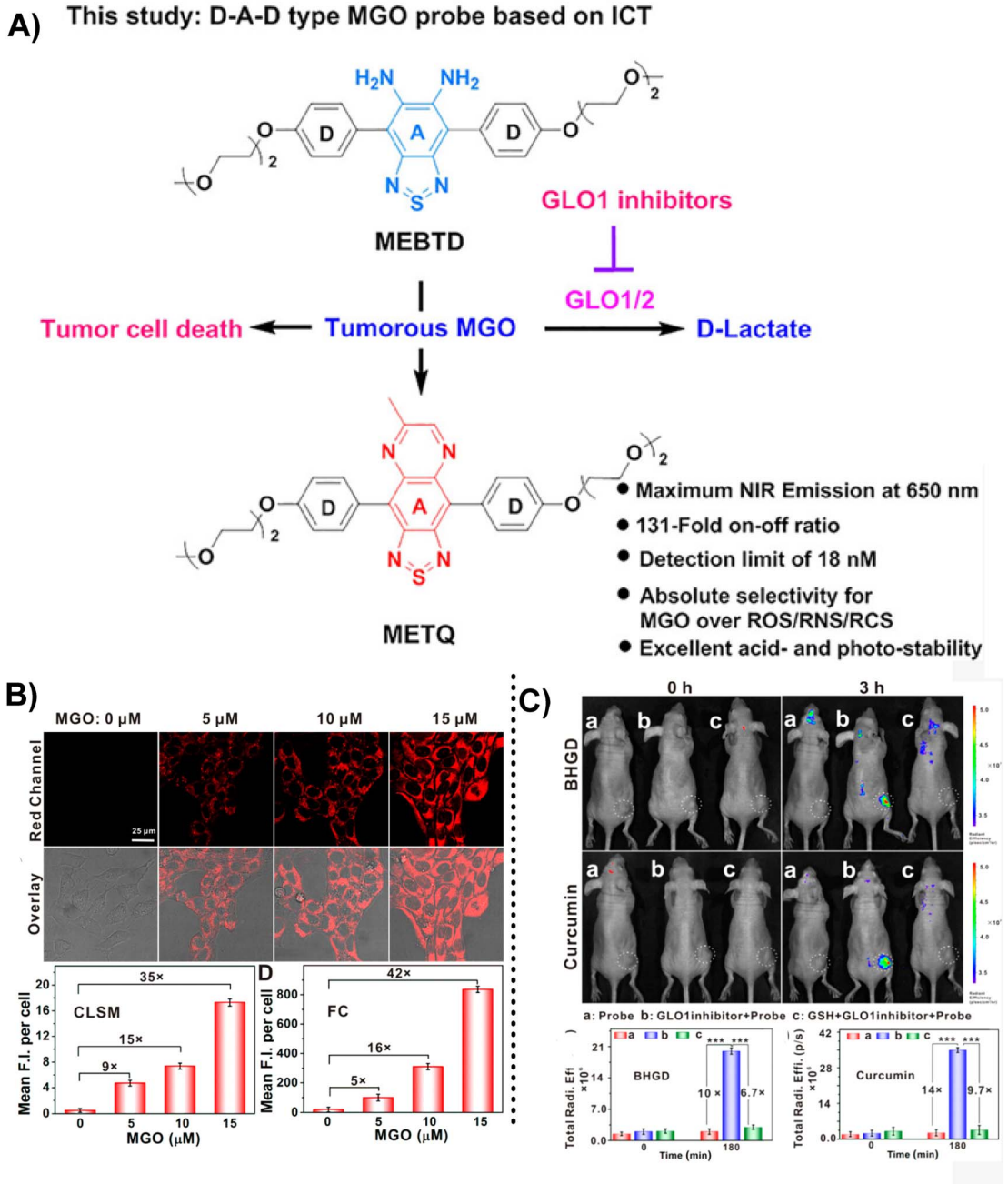

Fig. 15 (A) Recognition mechanism of MEBTD. (B) Fluorescence images of 4T1 cells using MEBTD at distinct MGO levels. (C) Fluorescence images of nude mice bearing 4T1 breast cancer xenografts with the injection of 100 μM of different GLO1 inhibitors. This figure has been reproduced from ref. 47 with permission from the American Chemical Society, copyright 2024.

a naphthalene-based probe utilized previously for NO quantification (Fig. 19A). However, even after increasing the NO concentration in the system to 200 μM, the fluorescence intensity of DAN remained essentially constant. In contrast to the probe that used OPD as the reactive group, DAN showed weak emission properties. There was a displacement of the fluorescence intensity peak with an increase in MGO content. DAN showed excellent performance and high sensitivity in the detection of RCSs, with a LOD value of 1.31 μM. Effective imaging of cancer cells by DAN provided a novel tool for tracking *in vitro* RCS levels.

However, DAN was unable to distinguish between FA, MGO, and GO; hence, they developed further improved probes. After a year of intensive effort, Jana *et al.*[25] created a water-soluble fluorescence probe, DAS, an ICT-based tool that was successful in identifying and differentiating between mono and dicarbonyl species. It featured a "D–π–A" structure, and the LOD of MGO shifted from 1.31 μM (DAN) to 33.4 nM. This probe was equally effective in real samples, such as raw fish and chicken,

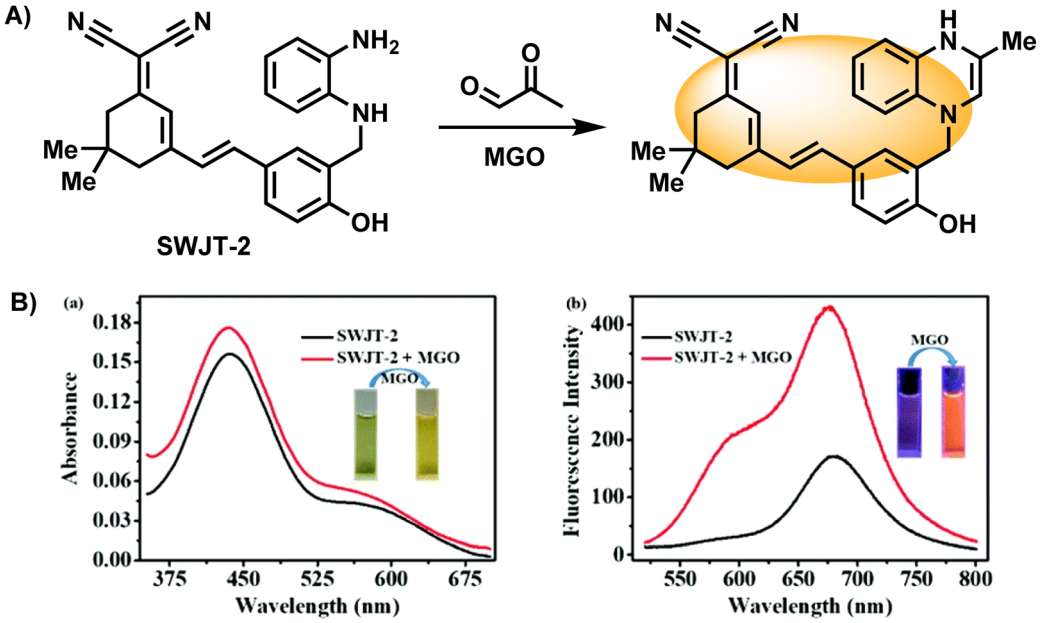

Fig. 16 (A) Recognition mechanism of SWJT-2. (B) Absorption and fluorescence spectra of SWJT-2 in DMF/PBS buffer solution. This figure has been reproduced from ref. 49 with permission from the American Chemical Society, copyright 2024.

and is regarded as an alternative to HPLC for testing MGO in Manuka honey at a reduced cost.

3.4. Guanidino (GND)

Instead of leveraging the specific reaction between the MGO and OPD, fluorescent probes can also be constructed based on the guanidino (GND) group. In 2021, Wang *et al.*[54] proposed a novel "AND"-logic-gate-based fluorescent probe with cell permeability (NAP-DCP-4) for detecting MGO level changes in activated macrophages *in vitro*. Different from most of the probes used to monitor MGO, the reactive group comprised two parts, OPD and GND, which emit fluorescence usually based on distinct response mechanisms. As seen in Fig. 20A, depending on whether these two sites participate in the reaction, the

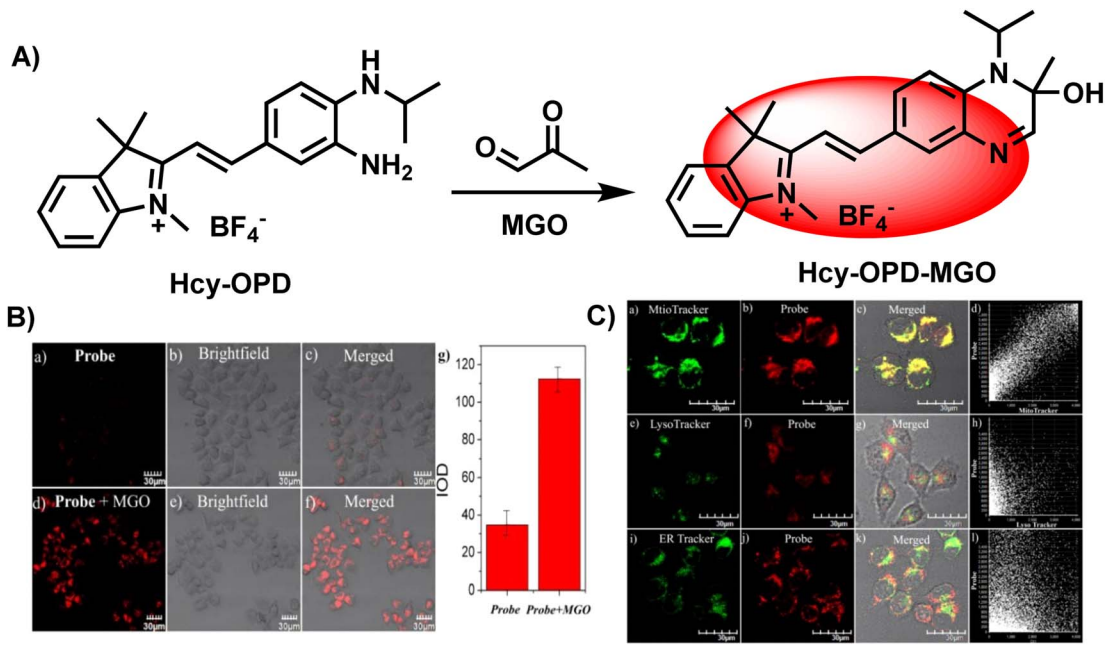

Fig. 17 (A) Recognition mechanism of Hcy-OPD. (B) Fluorescence imaging of zebrafish using Hcy-OPD with/without MGO. (C) Colocalization imaging of HeLa cells stained with Hcy-OPD. This figure has been reproduced from ref. 2 with permission from the Royal Society of Chemistry, copyright 2022.

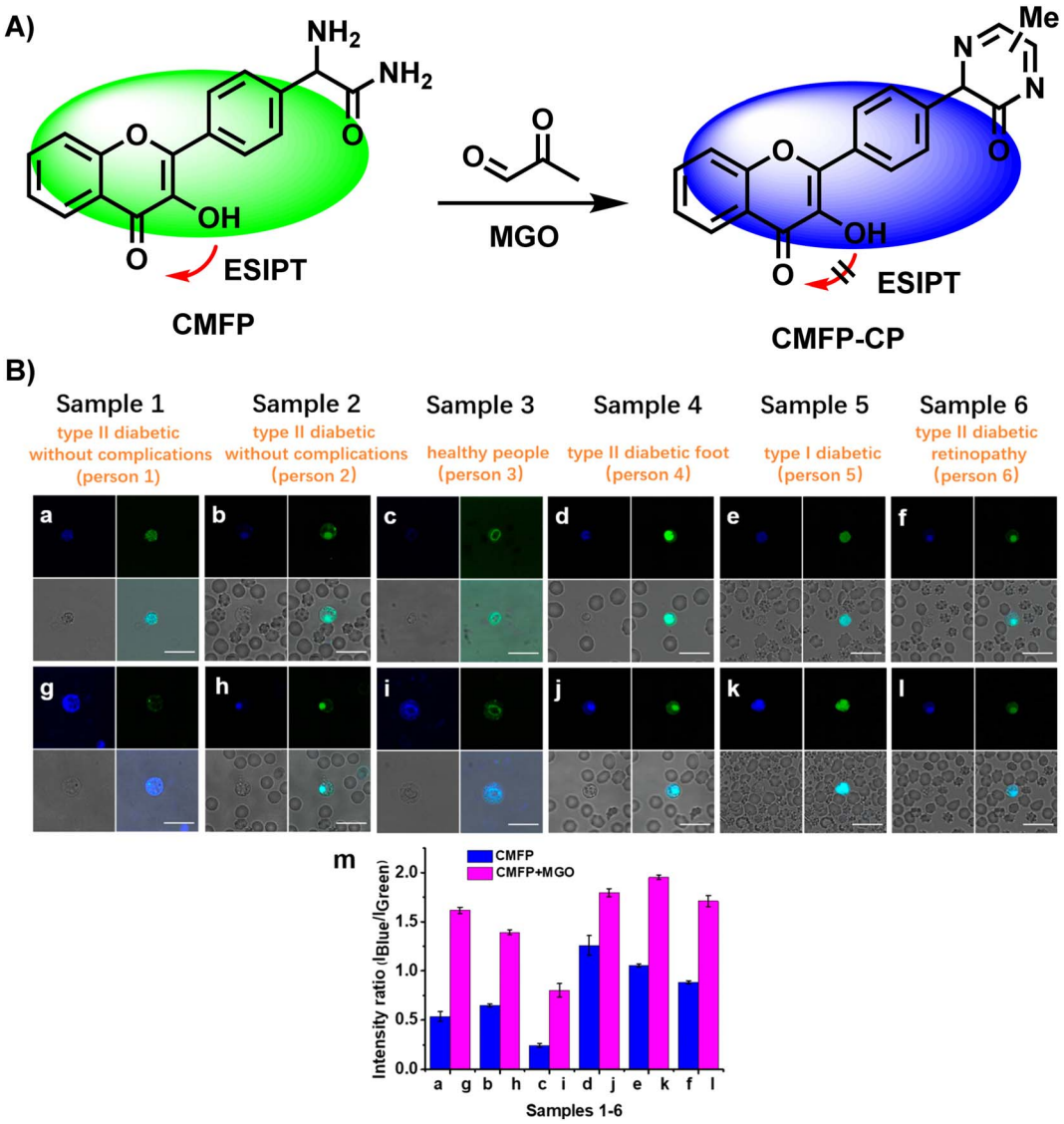

Fig. 18 (A) Recognition mechanism of CMFP. (B) Fluorescence images of 6 whole diabetic blood samples using CMFP. This figure has been reproduced from ref. 52 with permission from the American Chemical Society, copyright 2024.

results can be based on four random combinations, showing distinct fluorescence responses.

After a year, the same team reported ANC-DCP-1, a new probe that measures the concentrations of glyoxals (MGO and glyoxal, or GOS).[55] Notably, this probe also consisted of two recognition sites, OPD and GND. The dual reactive sites can help improve the selectivity for sensing a series of RCSs. Considering the suitability of NAP-DCP-4 in environments with pH values higher than 6.0, they chose 1,9-anthrenecarboximide as the fluorescent group to change the response conditions, providing a new tool for MGO detection in an acidic environment. It is hoped to be applied in diabetic urine samples that characterize a higher total GOS level and a pH of around 6.0. Testing MGO content in manuka honey can indirectly reflect the UMF scale in food, saving detection time. Nevertheless, both reports from this team do not address the imaging capabilities of the probe, and the ability to distinguish between MGO and GO, which warrants further investigation. The AND logic gate probe design principle has important implications for inspiring further probe development in the future.

4. Conclusion and outlook

An increasing number of publications in recent years have suggested a non-negligible association between MGO and numerous well-known illnesses. Sensitive and precise qualitative and quantitative measurement techniques are crucial for future pathological research. The superb optical characteristics, biocompatibility, and high sensitivity of fluorescent techniques have spurred their development in recent years. Their success at the animal level suggests that fluorescence probes may one day be used for disease diagnosis in humans. Reports on fluorescent probes for RCS have been growing ever since the first fluorescent probe was constructed by the Spiegel lab in 2013. This review is

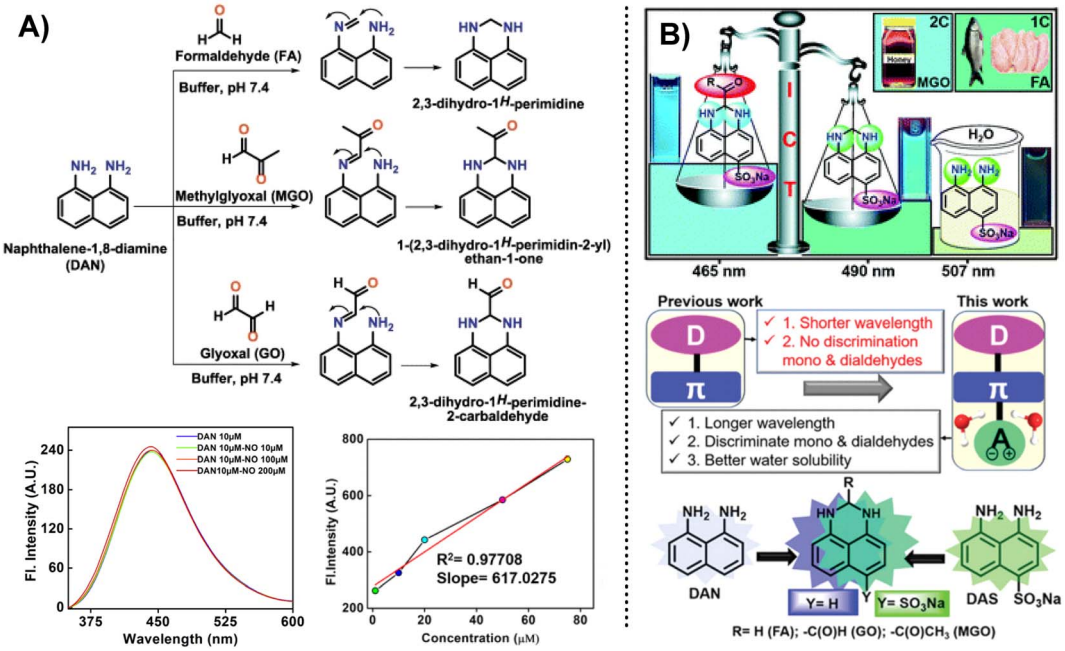

Fig. 19 (A) Detection mechanism of DAN (1,8-diaminonaphthalene) for sensing RCS. Reprinted from ref. 54, Copyright (2020), with permission from Elsevier. (B) Schematic of DAS and the comparison between DAN (1,8-diaminonaphthalene) and DAS. This figure has been reproduced from ref. 25 with permission from the Royal Society of Chemistry, copyright 2021.

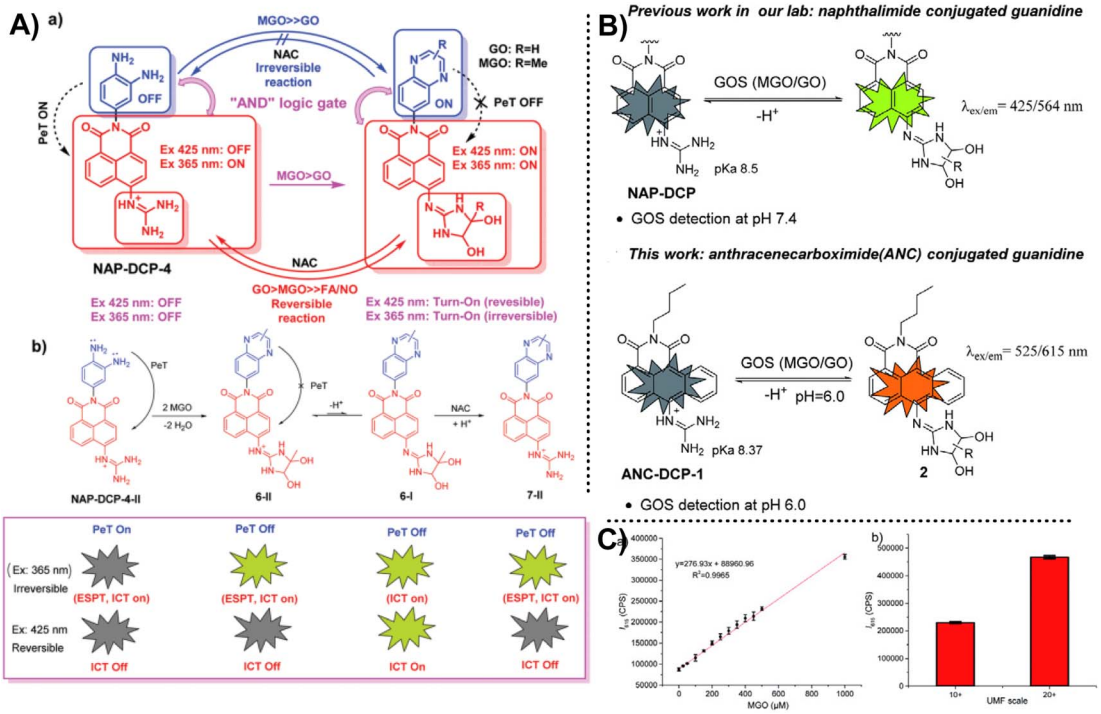

Fig. 20 (A) Detection mechanism of NAP-DCP-4. (B) Schematic of ANC-DCP-1 and the comparison between NAP-DCP and ANC-DCP-1. (C) Linear relationship between fluorescence intensity at 615 nm and MGO content. This figure has been reproduced from ref. 55 with permission from the Royal Society of Chemistry, copyright 2022.

mainly focused on the aforementioned fluorescent MGO probes, which are summarized in Table 1. The table presents a comparative analysis of various techniques employed for detecting MGO, highlighting key attributes, such as the probe type, response mechanism, limit of detection (LOD), response time, emission wavelength (λ_{em}), operational pH range, and imaging

Table 1 Performance comparison of techniques reported for the detection of MGO[a]

Probes	Response mechanism	LOD	Response time	λ_{em}/nm	Detection pH	Imaging application	Ref.
MBo	PET	50–100 nM	—	—	Physiological pH of 7.4	Imaging MGO in live HeLa cells	28
PDN-1	PET	77 nM	4–12 h	528	Physiological pH of 7.4	Two-photon imaging MGO in live HeLa cells	29
L	PET	—	About 30 min	620	Physiological pH of 7.4	Imaging exogenous MGO in L929 cells	30
NI-OPD	PET	56 nM	About 2 h	460	3.0–11.0	Two-photon imaging MGO in live HeLa cells, MCF-7 cells, in the kidney and liver tissues of diabetic mice	31
NP	PET	1.47 μM	About 40 min	555	4.5–10.0	Imaging MGO in living cells, tissues and zebrafish	32
DBTPP	ICT	262 nM	1.5 h	650	4.0–9.0	Imaging endogenous MGO in SH-SY5Y cells and transgenic AD mouse models	33
MGO-Naph-A	PET	1.36 μM	1 h	—	Physiological pH of 7.4	Imaging endogenous and exogenous MGO in A549 cells and zebrafish	34
TDTCD	ICT	57 nM	20 min	780–860	4.0–8.5	Imaging MGO in living mice	35
TM-IONPs	PET	72 nM	—	500–900	4.0–8.5	*In situ* NIR-II imaging of MGO in the brains of AD mice	36
ISP-MGO	ICT	2.18 ± 0.12 μM	8 min	—	7.0–8.0	Imaging endogenous and extracellular MGO in live cells	39
Cy-DNH2	ICF	95 nM	3 min	545	3.0–5.0	Imaging cellular MGO in the lysosomes of living cells and in the gastritis mouse model	40
D/I-PNTs	FRET	272 nM	—	820	6.5–6.8	*In vivo* imaging exogenous MGO in living 4T1 cells and 4T1 tumor-bearing mice	42
DAN (2,3-)	ICT	0.33 μM	1 h	—	Physiological pH of 7.4	Imaging exogenous MGO in living cells and *ex vivo* imaging MGO in the tissues of type II diabetes model mice	45
MEBTD	ICT	18 nM	1 h	650	4.0–9.0	Imaging MGO in Balb/c nude mice, tumor tissue and 5 cell with different glycolytic abilities	48
SWJT-2	PET	0.32 μM	15 min	674	7.4	Imaging endogenous and exogenous MGO in live HeLa cells 1	49
Hcy-OPD	PET	0.22 μM	1 h	658	7.0–7.4	Imaging MGO in live HeLa cells	2
CMFP	ESIPT	0.24 μM	About 40 min	—	Physiological pH of 7.4	Imaging endogenous MGO in living HeLa cells and whole blood samples from diabetic and healthy people	52
DAN (1,8-)	ICT	1.31 μM	2 h	350–600	4.5–7.4	Imaging MGO in live HeLa cells	53
DAS	ICT	33.4 nM	5 min	465	7.4	Imaging exogenous MGO in HepG2 cells and commercial manuka honey	25
NAP-DCP-4	PET	1.8 mM	—	559	7.4	—	54
ANC-DCP-1	ICT	7.3 μM	2 h	615	Around 6.0	—	55

[a] —: no relevant information.

applications. These techniques utilize diverse probes, predominantly based on PET, ICT, ESIPT, and FRET. The LODs vary significantly, with some probes capable of detecting MGO at nanomolar concentrations. Their response times range from minutes to hours, catering to different experimental requirements. The probes exhibit a broad spectrum of emission wavelengths, enabling imaging across various biological systems. The operational pH ranges encompass physiological and slightly acidic/alkaline conditions, suitable for different *in vitro* and *in vivo* imaging applications, including live cells, tissues, and animal models. However, the current MGO probes primarily utilize *o*-phenylenediamine as the recognition moiety. As reaction patterns continue to diversify, it is expected that more such groups capable of binding with MGO will emerge.

With increasing public emphasis on health, fluorescent probes are gaining more attention. Despite the considerable progress, several challenging issues still limit their use and remain to be solved; (1) commonly used probes are of lower-wavelength excitation and emission light, which limit their performance in intracellular detection and visualization. (2) Additionally, due to the complexity of real samples, the detection results are sometimes variable and unstable. (3) The auto-fluorescence of the scaffold interferes with the experimental results, especially when the color of fluorescence emission from the fluorophore is identical to that from the scaffold. However, two-photon fluorescent probes may help reduce the possibility of auto-fluorescence interference. Considering the first two points, the development of innovative ratiometric near-infrared or even multi-method combination fluorescent probes may be the focus of future research. Besides, to better understand the relationship between MGO and diseases, some scholars have studied the subcellular localization of probes, and the existing literature includes endoplasmic reticulum-targeting probes,[31] lysosome-targeting,[34,40] mitochondria-targeting probes.[2]

For *in vivo* fluorescence imaging, probes must exhibit high penetrability, good biocompatibility, stability across physiological pH levels, and low cytotoxicity parameters, which cannot be overlooked.[44] Despite recent advances, significant challenges remain before these probes can be used in biomedical applications in clinical practice. Current fluorescent probes available for MGO sensing and visualization offer real-time, non-invasive imaging capabilities, but face issues, such as limited tissue penetration and potential interference. Future research should focus on overcoming these challenges by developing probes with enhanced properties and validating their clinical relevance. With continued effort and improvement, we anticipate that these probes will showcase promising application prospects in the near future.

Data availability

Data sharing does not apply to this article as no new data were created or analyzed in this work.

Conflicts of interest

The authors declare that they have no competing interests.

Acknowledgements

This work was supported by Natural Science Foundation of China (NSFC, Grants 21605046) and Hunan Provincial Natural Science Foundation of China (No. 2017JJ3060 & 2023JJ30988).

References

1 A. N. Onyango, *Chem. Phys. Lipids*, 2012, **165**, 777–786.
2 Z. Wang, Y. Bian, C. Liu, S. He, L. Zhao and X. Zeng, *Chem. Commun.*, 2022, **58**, 6453–6456.
3 I. Allaman, M. Bélanger and P. J. Magistretti, *Front. Neurosci.*, 2015, **9**, 23.
4 P. Matafome, C. Sena and R. Seiça, *Endocrine*, 2013, **43**, 472–484.
5 J. Zheng, H. Guo, J. Ou, P. Liu, C. Huang, M. Wang, J. Simal-Gandara, M. Battino, S. M. Jafari and L. Zou, *Trends Food Sci. Technol.*, 2021, **107**, 201–212.
6 C. Angeloni, L. Zambonin and S. Hrelia, *BioMed Res. Int.*, 2014, **2014**, 238485.
7 D. Schumacher, J. Morgenstern, Y. Oguchi, N. Volk, S. Kopf, J. B. Groener, P. P. Nawroth, T. Fleming and M. Freichel, *Mol. Metab.*, 2018, **18**, 143–152.
8 L. R. Bhat, S. Vedantham, U. M. Krishnan and J. B. B. Rayappan, *Biosens. Bioelectron.*, 2019, **133**, 107–124.
9 T. Chang and L. Wu, *Can. J. Physiol. Pharmacol.*, 2006, **84**, 1229–1238.
10 X. Wang, K. Desai, T. Chang and L. Wu, *J. Hypertens.*, 2005, **23**, 1565–1573.
11 D. Talukdar, B. Chaudhuri, M. Ray and S. Ray, *Biochemistry*, 2009, **74**, 1059–1069.
12 C. Schalkwijk and C. Stehouwer, *Physiol. Rev.*, 2020, **100**, 407–461.
13 I. Nemet, L. Varga-Defterdarović and Z. Turk, *Clin. Biochem.*, 2004, **37**, 875–881.
14 E. Randell, S. Vasdev and V. Gill, *J. Pharmacol. Toxicol. Methods*, 2005, **51**, 153–157.
15 J. Zhang, H. Zhang, M. Li, D. Zhang, Q. Chu and J. Ye, *J. Chromatogr. A*, 2010, **1217**, 5124–5129.
16 S. Chatterjee, J. Wen and A. Chen, *Biosens. Bioelectron.*, 2013, **42**, 349–354.
17 A. Jana, M. Baruah and A. Samanta, *Chem.–Asian J.*, 2022, **17**, e202200044.
18 K. J. Bruemmer, T. F. Brewer and C. J. Chang, *Curr. Opin. Chem. Biol.*, 2017, **39**, 17–23.
19 F. Leblond, S. C. Davis, P. A. Valdés and B. W. Pogue, *J. Photochem. Photobiol., B*, 2010, **98**, 77–94.
20 B. W. Pogue, S. L. Gibbs-Strauss, P. A. Valdés, K. S. Samkoe, D. W. Roberts and K. D. Paulsen, *IEEE J. Sel. Top. Quantum*, 2010, **16**, 493–505.
21 S. Wang, W. X. Ren, J.-T. Hou, M. Won, J. An, X. Chen, J. Shu and J. S. Kim, *Chem. Soc. Rev.*, 2021, **50**, 8887–8902.
22 Y. Tang, Y. Ma, J. Yin and W. Lin, *Chem. Soc. Rev.*, 2019, **48**, 4036–4048.
23 X. F. Zhang and N. Feng, *Chem.–Asian J.*, 2017, **12**, 2447–2456.
24 W. Zhang, Z. Ma, L. Du and M. Li, *Analyst*, 2014, **139**, 2641–2649.

25 A. Jana, M. Baruah, S. Munan and A. Samanta, *Chem. Commun.*, 2021, **57**, 6380–6383.
26 H. Sahoo and J. Photoch, *Photobiol., C*, 2011, **12**, 20–30.
27 T. Ha, T. Enderle, D. Ogletree, D. S. Chemla, P. R. Selvin and S. Weiss, *Proc. Natl. Acad. Sci. U.S. A.*, 1996, **93**, 6264–6268.
28 T. Wang, E. F. Douglass Jr, K. J. Fitzgerald and D. A. Spiegel, *J. Am. Chem. Soc.*, 2013, **135**, 12429–12433.
29 T. Tang, Y. Zhou, Y. Chen, M. Li, Y. Feng, C. Wang, S. Wang and X. Zhou, *Anal. Methods*, 2015, **7**, 2386–2390.
30 C. Liu, X. Jiao, S. He, L. Zhao and X. Zeng, *Dyes Pigm.*, 2017, **138**, 23–29.
31 M. Yang, J. Fan, J. Zhang, J. Du and X. Peng, *Chem. Sci.*, 2018, **9**, 6758–6764.
32 S. Gao, Y. Tang and W. Lin, *J. Fluoresc.*, 2019, **29**, 155–163.
33 Y. Dang, F. Wang, L. Li, Y. Lai, Z. Xu, Z. Xiong, A. Zhang, Y. Tian, C. Ding and W. Zhang, *Chem. Commun.*, 2020, **56**, 707–710.
34 Z. Luo, Z. Zhu, T. Zhang, H. Jiang, N. Huang, F. Liang, Z. Wang, Y. Li, X. He and S. Qian, *Analyst*, 2022, **147**, 4949–4953.
35 Y. Dang, Y. Lai, F. Chen, Q. Sun, C. Ding, W. Zhang and Z. Xu, *Anal. Chem.*, 2022, **94**, 1076–1084.
36 Y. Lai, Y. Dang, Q. Sun, J. Pan, H. Yu, W. Zhang and Z. Xu, *Chem. Sci.*, 2022, **13**, 12511–12518.
37 M. HeeáLee and J. SeungáKim, *Chem. Soc. Rev.*, 2015, **44**, 4185–4191.
38 R. Gui, H. Jin, X. Bu, Y. Fu, Z. Wang and Q. Liu, *Coord. Chem. Rev.*, 2019, **383**, 82–103.
39 Z. Liang, Z. Jiang, C. Zhang and Z. Liu, *J. Mol. Struct.*, 2023, **1285**, 135484.
40 W. Xu, S. Liu, W. Cao and H. Xiong, *Sens. Diagn.*, 2024, **3**, 147–152.
41 Q. Xu, M. Ren, K. Liu, X. Wang, J.-Y. Wang, S. Wang and F. Kong, *Chem. Eng. J.*, 2022, **430**, 132851.
42 J. Liu, M. Li, Y. Dang, H. Lou, Z. Xu and W. Zhang, *Biosens. Bioelectron.*, 2022, **204**, 114068.
43 T. Ueno and T. Nagano, *Nat. Methods*, 2011, **8**, 642–645.
44 H. Kobayashi, M. Ogawa, R. Alford, P. L. Choyke and Y. Urano, *Chem. Rev.*, 2010, **110**, 2620–2640.
45 Q. Xie, Y. Zhan, L. Guo, H. Hao, X. Shi, J. Yang, F. Luo, B. Qiu and Z. Lin, *ChemistryOpen*, 2022, **11**, e202200055.
46 G. P. Ferguson, S. Tötemeyer, M. MacLean and I. R. Booth, *Arch. Microbiol.*, 1998, **170**, 209–218.
47 A. Bellahcène, M.-J. Nokin, V. Castronovo and C. Schalkwijk, *Semin. Cancer Biol.*, 2018, **49**, 64–74.
48 C. Ding, F. Wang, Y. Dang, Z. Xu, L. Li, Y. Lai, H. Yu, Y. Luo, R. Huang and A. Zhang, *Anal. Chem.*, 2019, **91**, 15577–15584.
49 H. Xu, X.-R. Liu, Z.-H. Cai, J. Zheng, Y.-W. Wang and Y. Peng, *Org. Biomol. Chem.*, 2022, **20**, 4782–4786.
50 Y. Li, Q. Chen, X. Pan, W. Lu and J. Zhang, *Top. Curr. Chem.*, 2022, **380**, 22.
51 L. Yuan, W. Lin, K. Zheng and S. Zhu, *Acc. Chem. Res.*, 2013, **46**, 1462–1473.
52 H. Wang, Y. Xu, L. Rao, C. Yang, H. Yuan, T. Gao, X. Chen, H. Sun, M. Xian and C. Liu, *Anal. Chem.*, 2019, **91**, 5646–5653.
53 A. Jana, M. M. Joseph, S. Munan, K. K. Maiti and A. Samanta, *J. Photochem. Photobiol., B*, 2020, **213**, 112076.
54 W. Wang, J. Chen, H. Ma, W. Xing, N. Lv, B. Zhang, H. Xu, W. Wang and K. Lou, *Chem. Commun.*, 2021, **57**, 8166–8169.
55 J. Chen, Y. Lin, W. Xing, X. Zhang, H. Xu, W. Wang and K. Lou, *RSC Adv.*, 2022, **12**, 9473–9477.